International Journal of Heat and Mass Transfer 217 (2023) 124634

Contents lists available at ScienceDirect

International Journal of Heat and Mass Transfer

journal homepage: www.elsevier.com/locate/ijhmt

Frictional resistance investigation of sCO_2 and a semi-empirical friction factor correlation based on wall-of-the-law

Zheng Wang [a,b], Qinghe Guo [a,b], Yi Wu [a,b], Zhangquan Wen [a,b], Yafei Liu [a,b], Dan Chen [a,b], Peiwang Zhu [a,b,*], Gang Xiao [a,b,*]

[a] Key Laboratory of Clean Energy and Carbon Neutrality of Zhejiang Province, Zhejiang University, Hangzhou, Zhejiang 310027, China
[b] State Key Laboratory of Clean Energy Utilization, Zhejiang University, 38 Zheda Road, Hangzhou 310027, China

ARTICLE INFO

Keywords:
Supercritical CO_2
Isothermal and non-isothermal
Density fluctuation
Law-of-the-wall
Friction factor correlation

ABSTRACT

The flow resistance characteristics of variable property fluids, particularly supercritical fluids, such as supercritical CO_2 (sCO_2), play a crucial role in the design, operation control, and simulation of energy systems. However, drastic changes in thermophysical properties near the pseudo-critical regime under various boundary conditions make it challenging to find suitable theoretical and correlation models that can accurately predict their friction factors.

In this study, the experimental investigations on the frictional resistance characteristics of upward sCO_2 flow under different heat flux and tube wall roughness is conducted. The results show that as the heat flux increases, sCO2′s friction factor decreases under the same reference temperature, and the decrease becomes less significant with increasing tube wall roughness. The *SST k-ω* simulation attributes this phenomenon to the suppressed sensitivity of turbulence velocity fluctuations to thermal boundary conditions in high roughness pipes. Additionally, the experiment shows that near the pseudo-critical point, sCO2′s friction factor abnormally increases, which can be reasonably explained by the density fluctuation theory. A new semi-empirical expression for the variable property fluid's friction factor by combining the law-of-the-wall is derived for the first time, and the correlation is regressed based on the experimental and literature results. The new correlation exhibits good predicting performance, with 94% of predictions falling within ±20% absolute deviation from the original experimental results. This result confirms consistent flow resistance characteristics between supercritical flow and subcritical single-phase flow.

1. Introduction

Supercritical CO_2 (sCO_2) is a promising working fluid that can play an important role in various fields, including supercritical extraction [1], supercritical cleaning [2], advanced heat pump systems [3], and advanced energy systems [4,5]. Due to the demand for promoting energy efficiency and reducing greenhouse gas emissions, the application of sCO_2 in advanced energy systems has received particular attention. The sCO_2 Brayton cycle is applicable to a variety scenarios such as nuclear power, fossil fuel power and concentrated solar power due to its high efficiency, faster load regulation [6] and applicability to dry cooling [7]. The transcritical CO_2 (tCO_2) heat pump is also highly significant, with characteristics such as low greenhouse gas emissions and excellent heating performance making it suitable for use in mobile air conditioning systems [8] or the production of hot water instead of conventional industrial waste heat boilers [9]. In sCO_2 thermodynamic systems, CO_2 typically undergoes complex state changes during system start-up, shut-down, load variation, and even under normal operations. Therefore, accurately understanding the flow resistance characteristics of sCO_2 will provide important guidance for pipe design, system operation control, equipment over-temperature protection, and system dynamic modeling. It will also offer valuable reference for the applications of other supercritical fluids. However, due to the complex thermophysical property variation near the pseudo-critical point, accurately predicting the pressure drop characteristics of variable property fluids over a wide range is usually a challenging task [10].

The study of frictional pressure drop in single-phase fluids can be traced back more than a century. In 1883, Reynolds [11] used the similarity principle to obtain the Reynolds number (*Re*), which represents the flow instability, providing a solid foundation for subsequent research on hydraulic characteristics of pipe flows. In 1912, Blasius

* Corresponding authors.
E-mail addresses: zhupw@zju.edu.cn (P. Zhu), xiaogangtianmen@zju.edu.cn (G. Xiao).

https://doi.org/10.1016/j.ijheatmasstransfer.2023.124634
Received 27 May 2023; Received in revised form 23 July 2023; Accepted 23 August 2023
Available online 4 September 2023

Nomenclature

Latin Alphabet

AP	acid passivation
AU	average uncertainty
B	constants in the logarithmic velocity law-of-the-wall.
d	tube diameter [m]
DC	direct current
EP	electrolytic polishing
f	friction factor
I	turbulence intensity
L	length [m]
MAD	mean absolute deviation
MAE	average absolute error
MU	maximum uncertainty
R	tube radius [m]
RANS	Reynolds-averaged Navier-Stokes equations
RMSE	root mean square error
R_{zd}	mean peak-to-valley height, which is used to quantify surface roughness [μm]
sCO_2	supercritical CO_2
SQP	Sequential Quadratic Programming
T	temperature [°C]
tCO_2	transcritical carbon dioxide
u *or* U	velocity [$m{\cdot}s^{-1}$]
u^+	dimensionless velocity
$\overline{u'v'}$	turbulent velocity fluctuations [$m^2{\cdot}s^{-2}$]
y^+	dimensionless wall-normal distance

Greek Letters

ΔP	differential pressure
ε	roughness height [μm]
κ	constants in the logarithmic velocity law-of-the-wall.
μ	dynamic viscosity [Pa·s]
ρ	density [$kg{\cdot}m^{-3}$]
τ	shear stress [$kg{\cdot}m^{-1}{\cdot}s^{-2}$]

Subscripts

axis	parameters at the central axis of the tube
b	bulk fluid
f	frictional
pc	parameters at pseudo-critical point
r	parameters at reference state
VD	Van Driest transformation
w	parameters at the wall
τ	parameters at wall shear layer
∞	parameters of the mainstream/bulk fluid

Dimensionless numbers

Re	Reynolds number
*Re**	roughness Reynolds number
Ri	Richardson number

[12], combining existing experimental data, proposed the classical −1/4 power-law correlation for the smooth tube friction factor. In 1933, Nikuradse [13] create artificially rough tubes by attaching sand grains to the tubes' inner wall and investigated the influence of pipe roughness on friction factors. Based on the effect of roughness height on the viscous sublayer, Nikuradse divided the law-of-resistance into three ranges. Subsequently, Colebrook et al. [14], combining Nikuradse's experimental results with Prandtl's logarithmic velocity law [15], obtained a satisfactory friction factor correlation for rough tubes. Many scholars have made further improvements and studies on the friction factors of single-phase fluids in smooth and rough pipes, which are well summarized in the work of Wang et al. [16].

Although the case of single-phase fluid flow is relatively simple and has been studied by many researchers for a long time, the situation will be significantly different when there are thermal boundary conditions. Allen [17] experimentally studied the characteristics of flow resistance of water at 0.5 MPa in a horizontally straight tube under uniform heat flux boundary. It was found that the friction factor of water decreases as the wall temperature increases (i.e., the heat flux increases). It is worth noting that when he used wall temperature as the reference viscosity to calculate the *Re*, the results of the friction factor can better satisfy the Blasius correlation. Carr et al. [18] experimentally measured the velocity and turbulence intensity distribution of upward air flow under heating conditions. It was found that with the increase of heat flux, the turbulence intensity and turbulent shear stress show a significant decreasing trend, but the friction factor seems to decrease first and then increase with the increase of heat flux. Easby [19] experimentally studied the frictional resistance characteristics of nitrogen at 0.4 MPa in the downward flow under heating conditions. He found that the friction factor shows a uniform decreasing trend as the Richardson number (*Ri*) increases (i.e., the wall heat flux increases). According to his measurement results of flow field parameters, he believes that the decrease of the friction factor is due to the decrease of the turbulence shear stress in the tube.

For supercritical fluids, due to the drastic variations in thermophysical properties especially near the pseudo-critical point, their frictional resistance characteristics often exhibit more complex patterns. Pioro et al. [10] conducted a survey of the research on flow resistance of supercritical fluids. The conclusion was that because of the steep variation in fluid's thermophysical properties at high heat flux under supercritical pressure, there were no analytical and numerical methods available at that time that could accurately predict the pressure drop characteristics of supercritical fluids. However, they also indicated that the total pressure drop of supercritical fluids can be unified with the pressure drop for subcritical fluids by introducing property correction factors.

Pettersen et al. [20]conducted experimental research on the flow resistance of sCO_2 under cooling conditions in 0.787 mm microtube. They found that the Blasius correlation slightly underestimated the pressure drop of sCO_2 while the Colebrook correlation could perfectly predict the experimental results if the tube roughness was assumed to be 1 μm. However, it is important to note that their experimental results did not exclude the pressure drop due to flow acceleration. Liao and Zhao [21] experimentally investigated the pressure drop characteristics of sCO_2 during cooling conditions in tubes ranging from 0.5 ~ 2.16 mm. Their results indicated that the pressure drop tended to decrease as the tube diameter decreases, while the pressure drop remained relatively stable with changing *Re*. However, they only corrected the dynamic pressure loss but not the acceleration pressure drops. Yamashita et al. [22] experimentally investigated the flow resistance of vertically upward heating flow of supercritical R22 in a 4.4 mm tube. They observed a significant decrease in the friction factor of R22 near the pseudo-critical point as the heat flux increased, which they attributed to the significant reduction in the fluid's viscosity near the heated wall. Jiang [23] experimentally investigated the pressure drop of supercritical R404 during cooling conditions in a horizontal 9.4 mm tube. He found that the friction factor of R404 continuously decreased as the *Re* increases, and there was a noticeable increase in the friction factor near the critical point in his experiment data. By dividing the supercritical regime into three regions and modifying the Churchill's correlation [24] with property ratio terms and diameter ratio term, a suitable friction factor correlation was derived for his operating conditions, which can

effectively control the prediction deviation of 90% of his experimental data within a range of ±15%. This pattern of correlation was also adopted by Andresen et al. [25]. Jiang et al. [26] demonstrated that the friction pressure drop of supercritical R134a cooling in a horizontal 4.01 mm tube significantly increased as the pressure approached the critical pressure. By implementing Petrov and Popov's correlation [27], along with property correction terms and heat flux correction term, they obtained a correlation that accurately predicted their experimental results, typically within a deviation of ±20%. Zhang et al. [28] reported quite different results from previous studies regarding the adiabatic pressure drop test of RP3. They discovered that the friction factor of supercritical RP3 near and above the pseudo-critical point would be dramatically different from that of conventional fluids, even with an increase in the friction factor as *Re* increases. Wang et al. [16] conducted experimental research on the adiabatic flow resistance of sCO_2 in roughness tubes, while accounting for the effect of tube roughness. They proposed a friction factor correlation that could more accurately predict their experimental results compared to other known correlations. The predicted accuracy under low *Re* conditions can reach ±0.98%, which is significantly lower than the ±5.68% of the Colebrook correlation. Fang et al. [29]systematically summarized previous research results on supercritical flow resistance and derived a better correlation for the friction factor of supercritical adiabatic flow in rough pipes by incorporating a new dimensionless number, and can predict 87.7% of their collected data within ±20%.

In recent years, some researchers used the analogy of subcritical two-phase flow theory to study the flow resistance characteristics of supercritical flow. Zhang et al. [30]analogized subcritical evaporation process [31] and proposed a new dimensionless number to include the relative effects of the induced force of "pseudo-evaporation" provided by wall heat flux to fluid inertia force. The new correlation provides an effective prediction of their experimental results, with a mean absolute relative error of 18.1% and a root-mean-square relative error of 21.2%, which exhibits significantly lower deviation compared to other correlations evaluated by them. Hao et al. [32]developed a friction factor correlation that incorporates "Pseudo-vapor mass quality" by introducing the supercritical three-regime model [33]. The correlation was well validated against their experimental results, demonstrating a mean absolute relative error of 9.02% and a root mean square error and 10.74%. However, further experimental results are still needed to verify the rationality and necessity of the supercritical two-phase analogy. In addition, Zhu et al. [34]derived a new dimensionless number, which signifies the relative effects of thermal-induced force and fluid inertia force, by combining a simple dimensionless analysis method. They obtained a correlation that satisfied their experimental values well with a mean absolute relative error of 6.67% and a root mean square error and 8.71%, by combining Filonenko correlation [35], property correction terms, and the new dimensionless number correction terms.

After summarizing and contemplating the current research results, it has been found that most researchers' experimental operating conditions are relatively narrow. The correlations obtained are usually only applicable to their own experimental results and therefore lack generality. Furthermore, the vast majority of researchers have not considered the wall roughness effect, and the friction factor correlation lacks theoretical guidance and is only empirical in nature. Therefore, a systematic investigation into the frictional resistance law of supercritical fluids with regard to wall roughness effects and thermal boundary conditions is necessary.

However, there are more profound considerations regarding supercritical frictional resistance when combined with current literature conclusions. Considering Allen's conclusion [17] that even conventional fluids such as water exhibit a characteristic of decreasing friction factor with increasing heat flux, which is similar to the heating results of supercritical flow [22]. This likely suggests that supercritical flow possesses properties similar to subcritical single-phase flow. Therefore, it is possible to explore a combined theory that links these two phenomena.

Based on the aforementioned deficiencies and considerations, this study conducted an experimental investigation of frictional characteristics of isothermal and non-isothermal upward flow of sCO_2 in vertical tubes with different surface roughness. By comparing the results with simulations, we identified the limitations of the current Reynolds-averaged Navier-Stokes equations (RANS) simulations in predicting near-critical flow behaviors. Furthermore, we used the critical density fluctuation theory to reasonably explain the anomalous behavior of friction factors near the pseudo-critical point. Finally, based on the law-of-the-wall and reasonable assumptions, we derived a semi-empirical correlation to predict the friction factors of fluids with variable properties under isothermal or non-isothermal conditions. This result is expected to contribute to further understanding the unified nature of friction factors in subcritical single-phase flow and supercritical flow.

2. Experimental parts

2.1. Experimental facility

The flow resistance experiment was conducted on a tCO_2 system located at Qingshanhu Energy Research Center of Zhejiang University. As shown in Fig. 1, the experimental system primarily consists of a CO_2 liquid storage tank, a plunger-type booster pump, a helical coil direct current (DC) electrical preheater, a vertical DC electric heated section (i.e., the experimental section), an electronically controlled slide-type pressure regulating valve, and two shell-and-tube heat exchangers.

Before the operation of experiment, the CO_2 with a purity of 99.9% is injected into the tCO_2 circulation loop from CO_2 liquid storage tank by a charging pump. The liquid CO_2 in the loop is then pressurized by the plunger pump to start the circulation process. The inlet temperature of the test section is regulated by adjusting the DC voltage (i.e., heating power) of the preheater. The vertically test section is made up of 316 L stainless steel, wherein the wall heat flux is also regulated by adjusting the DC voltage. The entire tube is covered by a 100 mm thermal insulation layer. The pressure of the test section is controlled by pressure regulating valve. Numerous studies have demonstrated that the presence of lubricating oil significantly increases the frictional pressure drop of sCO_2 [36–38]. The reciprocating plunger pump inevitably requires lubricating oil for its reciprocating motion, which may potentially introduce lubricating oil into the system pipeline. Considering that the process of lubricating oil entering the pipeline from the plunger pump is typically very slow and its accumulation effect is often more pronounced, in addition to the fact that the operating pressure of the oil separation device is usually low, we finally decided to place the oil separator at the low-pressure side of the system instead of directly at the outlet of the pump. So, after being throttled by pressure regulating valve, the gaseous CO_2 firstly enters the oil separator for filtration, then passes through two stages of shell-and-tube water coolers to cool down into a subcooled liquid state, and finally returns to the booster pump.

The mass flow rate of the experimental loop is measured using a Coriolis-type mass flowmeter installed at the outlet of the booster pump. At the inlet of the test section, a pressure transmitter is installed to monitor the inlet pressure. Additionally, a differential pressure transmitter is employed to monitor the pressure drop across the test section. Two T-type thermocouples are placed at the inlet and outlet of the test section, calibrated against a first-grade precision standard mercury-in-glass thermometer within the temperature range of 10 ~ 80 °C and are considered to have a measurement deviation of ±0.3 °C. Furthermore, seventeen clamp-on K-type thermocouples are uniformly distributed along the outer surface of the test section to monitor the outer wall temperature of the tube. Due to the relatively long length of the test section and the vertical upward flow of the fluid, the combined effects of gravity, flow resistance, and momentum loss during acceleration can result in slightly lower temperatures at the outlet compared to the inlet. Therefore, a special average of the inlet and outlet temperatures is used to represent the reference temperature of the test section. This aspect is

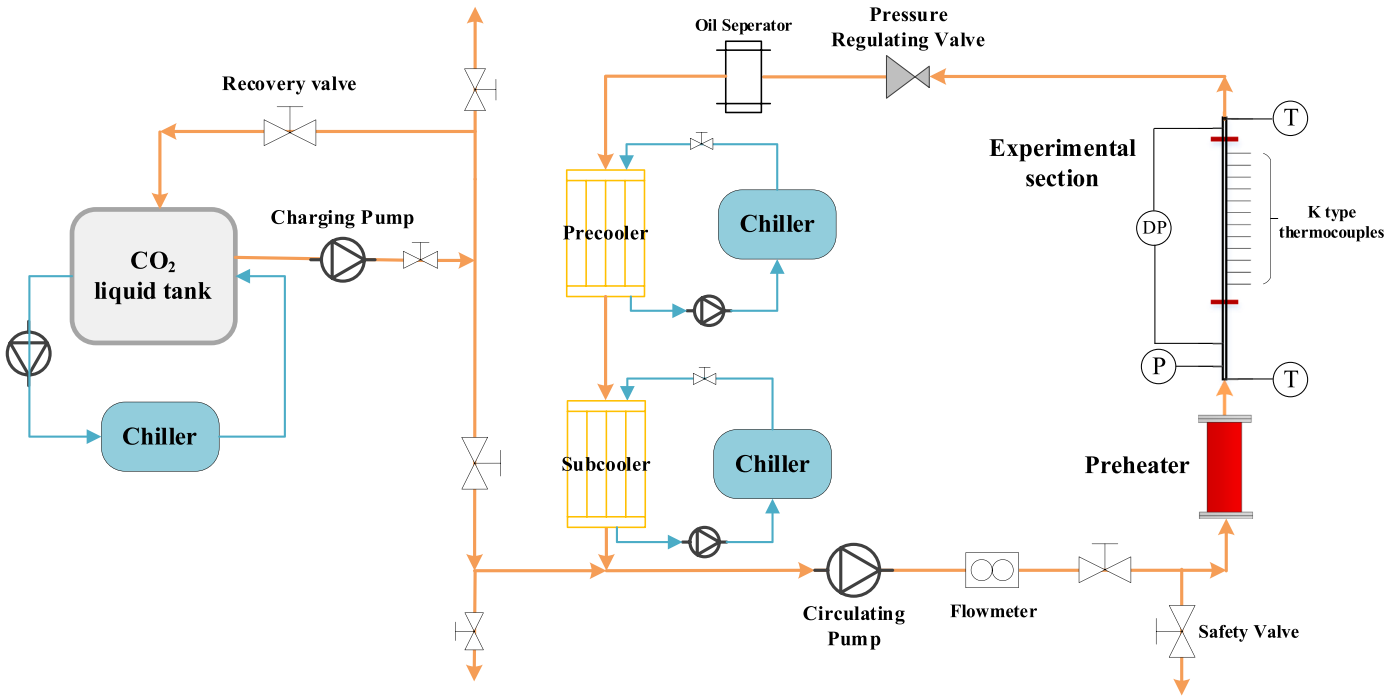

Fig. 1. The flowchart of experimental system.

discussed in more detail in Section 3.3 of this paper and Chapter 3 of the supplementary information (it should be noted that this approach is not only applied to heating conditions but also to adiabatic conditions.). These K-type thermocouples were calibrated at room temperature for their temperature reference point, using a standard mercury thermometer. The signals from all instruments are collected by the HollySys® automation system, which uploads the processed data to the computer terminal. To minimize deviations caused by signal fluctuations originating from environmental or equipment factors, the data for each experimental condition is averaged over a period of 30 s (with a sampling interval of 0.5 s).

The pressure drop experiment was conducted using two specifications of 316 L stainless-steel tubes. Tube A, underwent electrolytic polishing (EP), resulting in relatively low surface roughness. Tube B, on the other hand, underwent acid passivation (AP), leading to relatively higher surface roughness. The surface roughness of both tubes was measured using the TR200 handheld surface roughness instrument. R_{zd} is a significant roughness parameter affecting fluid flow [39]. Adams et al. [40] proved that R_{zd} is a roughness parameter that closely approximates sand-grain roughness. Thus, in our experiment, the roughness of the tubes is determined based on the measured R_{zd} values. The specific parameters of the tubes are presented in Table 1.

A preliminary heat balance experiment was conducted using Tube A as a reference, in which a comparison was made between the heat input from the DC power source and the calculated fluid heat absorption rate at conditions far from the pseudo-critical point. The results are presented in the Fig. 2. The mean absolute deviation (MAD) between the calculated heat flux and the input heat flux was found to be 5.14 kW·m^{-2}, indicating a satisfactory insulation effect of the test section. Therefore, the test section is considered to be well insulated.

Table 1
The tubes' size parameters.

Tube A		Tube B	
outside diameter / mm	12.7	outside diameter / mm	12.7
inside diameter / mm	9.4	inside diameter / mm	10.2
entrance length / mm	420	entrance length / mm	466
heated length / mm	2340	heated length / mm	2304
outlet length / mm	115	outlet length / mm	120
R_{zd}/ μm	1.440	R_{zd}/ μm	19.428

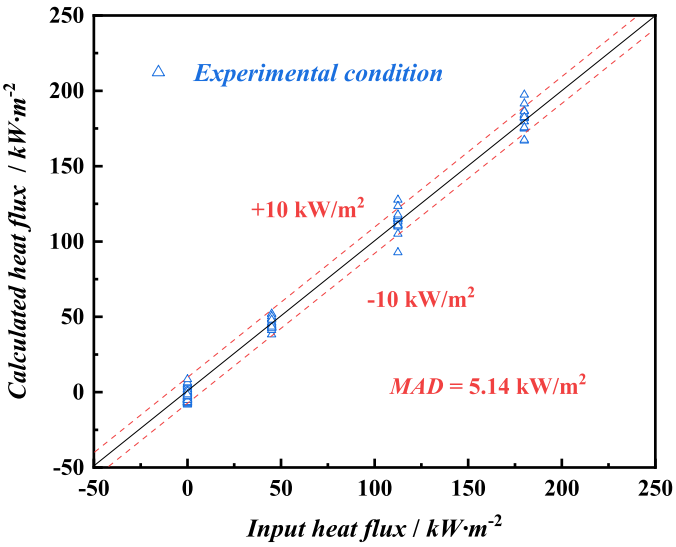

Fig. 2. Heat balance test of the experiment section (MAD means "mean absolute deviation").

2.2. Data processing methods

In this experiment, it is necessary to account for gravity-induced pressure drop as the fluid flows vertically upward. Furthermore, the acceleration pressure drops along the tube and the local pressure drop at the tee-tube junction is also need to be corrected. A comprehensive analysis of data processing methods and some key operational procedure in experiments are provided in detail in *Supplementary Information Chapter 1*.

2.3. Uncertainty analysis

The Type B uncertainty arising from measurement errors of the instruments is presented in Table 2. The average uncertainty (AU) and maximum uncertainty (MU) of the main calculated results in our experiment are presented in the Table 3. The maximum uncertainty occurs near the pseudo-critical point, which is attributed to the significant impact of temperature on the thermophysical properties. Error bars have been incorporated into all experimental results to indicate the specific uncertainties associated with each condition. For the detailed process of uncertainty calculation, please refer to *Supplementary Information Chapter 2*.

3. Numerical methods

3.1. Physical model construction

The simulation in this study was conducted using the ANSYS Fluent software. The physical model is shown in the Fig. 3(a). Only the CO_2 domain was considered in simulation. All physical dimensions of the tube are designed to be the same as the actual experimental values. Structured O-type meshes were generated using the Integrated Computer Engineering and Manufacturing code for Computational Fluid Dynamics (ICEM CFD). Taking Tube A as an example, the cross-sectional mesh and volume mesh are shown in Fig. 3(b). It should be noted that when the surface roughness is significant, R_{zd}, which representing the actual tube roughness effect, may deviate from the idealized "sand grain roughness". This is proved both on Adams' work [40] and our preliminary simulations. Therefore, in the simulation, the roughness of Tube B is not set to be the same as the actual experimental value, but to a relatively larger value than that of Tube A.

3.2. Numerical model validation and mesh independence check

Tube A at an inlet condition of 7.6 MPa and a mass flow rate of 0.125 $kg{\cdot}s^{-1}$ was selected to perform the mesh independence check. For tubes with rough surfaces, the roughness Reynolds number (Re^*) is used to evaluate the impact of roughness height on tubes, as defined by Eq. (1).

$$\mathrm{Re}^* = \frac{\rho u_\tau \varepsilon}{\mu} \tag{1}$$

Where ρ is the density of fluid; u_τ is the wall shear velocity; ε is the roughness height; μ is the dynamic viscosity of fluid. The expression for u_τ can be given as Eqs. (2) ~ (3).

$$u_\tau = \sqrt{\frac{\tau_w}{\rho}} \tag{2}$$

$$\tau_w = \frac{f \rho U_\infty^2}{2} \tag{3}$$

Where τ_w is the wall shear stress; f is friction factor; U_∞ is the bulk fluid velocity.

The friction factor can be approximated using the Blasius correlation,

Table 2
Experimental instrument and their *Type B* uncertainty.

Instrument	Measured parameter	Range	Uncertainty
flowmeter	mass flow rate	0 ~ 0.3 $kg{\cdot}s^{-1}$	±0.2% FS
pressure transmitter	inlet pressure	-0.1 ~ 25 MPa	± 0.075% FS
differential pressure transmitter	differential pressure	-100 ~ 500 kPa	± 0.075% FS
T-type thermocouple	inlet/outlet temperature	0 ~ 200 °C	± 0.3 °C
K-type thermocouple	wall temperature	0 ~ 600 °C	± 1.5 °C

Table 3
The uncertainty of the main parameters.

Tube A			Tube B		
	AU%	MU%		AU%	MU%
pressure drop	4.5	25.2	pressure drop	4.0	24.4
Re	2.3	18.7	*Re*	2.5	21.3
friction factor	5.0	29.5	friction factor	4.7	25.6

which would not result in a significant deviation. Considering the *Re* range of $10^5 \sim 10^6$ in our experiment, by substituting the roughness height and other parameters into Eq. (1) ~ (3), the resulting value of Re^* falls within the range of 1.64 ~ 14.86, with an average value of 6.13. Generally, when Re^* is below 2, the tube wall is considered smooth [41]. Some researchers have also considered a criterion of 5 [28,42]. Regardless of which criterion is used, Tube A cannot be simplified as a smooth pipe. Therefore, in the simulation, an equivalent sand-grain roughness of 1.44 μm is set to represent the roughness of Tube A.

To ensure sufficient grid refinement, the center height of the first grid layer near the wall is set to satisfy $y^+<0.5$. Three sets of meshes are generated based on different y^+ levels, axial grid density, and radial grid density, with grid quantities of 829,400, 1,612,800, and 2,662,200, respectively. The thermophysical properties of CO_2 are obtained from the NIST database imbedded in the ANSYS Fluent software, and interpolation tables are generated, with pressure interval of 0.01 MPa and temperature interval of 0.1 K. To reduce numerical errors, the operating pressure is set to the inlet pressure of the tube. The inlet and outlet of the tube adopt mass flow rate boundaries. The turbulence intensity (I) at the tube inlet is set using the assumption of fully developed turbulent flow, which can be expressed as $I = 0.16{\cdot}\mathrm{Re}^{-0.125}$. The entrance and outlet sections are treated as adiabatic wall boundaries, and the heated section is subjected to a uniform heat flux boundary. To account for the gravity-induced pressure drop in the vertical direction, the operating density is set to zero. The initial calculation is performed using the SIMPLEC algorithm with low-order discretization and 50 pre-computed steps. Then, the solver is switched to the COUPLED algorithm with second-order discretization. The solution process is considered to be converged when the residuals of all parameters reach 10^{-5}.

Four numerical models were selected: Standard k-ε [43], RNG k-ε [44], Realizable k-ε [45], and SST k-ω [46]. These models were chosen because of their capability to solve rough wall flow. The wall temperature distribution and total frictional pressure drop of the tube obtained from the simulations are shown in Fig. 4. From the results in Fig. 4(a) ~ (d), it can be observed that all models for both operating conditions exhibit mesh independence for the three mesh sets. In Fig. 4(a), it can be seen that when the heat flux is relatively low and the temperature is above the pseudo-critical point, all four models provide good predictions in wall temperatures. In Fig. 4(b), it is observed that the predicted pressure drops also show good agreement with the experimental values. However, in Fig. 4(c), when the heat flux is relatively high and the temperature is below the pseudo-critical point, all four models exhibit a deviation of approximately 20 K from the experimental wall temperature. Additionally, all three k-ε models showed unphysical solutions for the wall temperature distribution. Only the SST k-ω model can capture the same trend of wall temperature distribution. Considering that the SST k-ω model provides the most reasonable results, it is adopted for the subsequent simulations in our study.

To evaluate the impact of inlet turbulence intensity on the simulated ΔP_f, we conducted simulations for a typical adiabatic condition (7.6 MPa, 1801 $kg{\cdot}m^{-2}{\cdot}s^{-1}$, 0 $kW{\cdot}m^{-2}$) with various levels of inlet turbulence intensity. For this operating condition, the calculated turbulence intensity level for fully developed turbulent flow ranged from 2.9% to 3.5%. Hence, we compared the original simulation results with cases in which the inlet turbulence intensities were set to 1% and 5%. As shown in Fig. 5, when the inlet turbulence intensity varies between 1% and 5%, the simulated frictional pressure drop exhibits negligible differences,

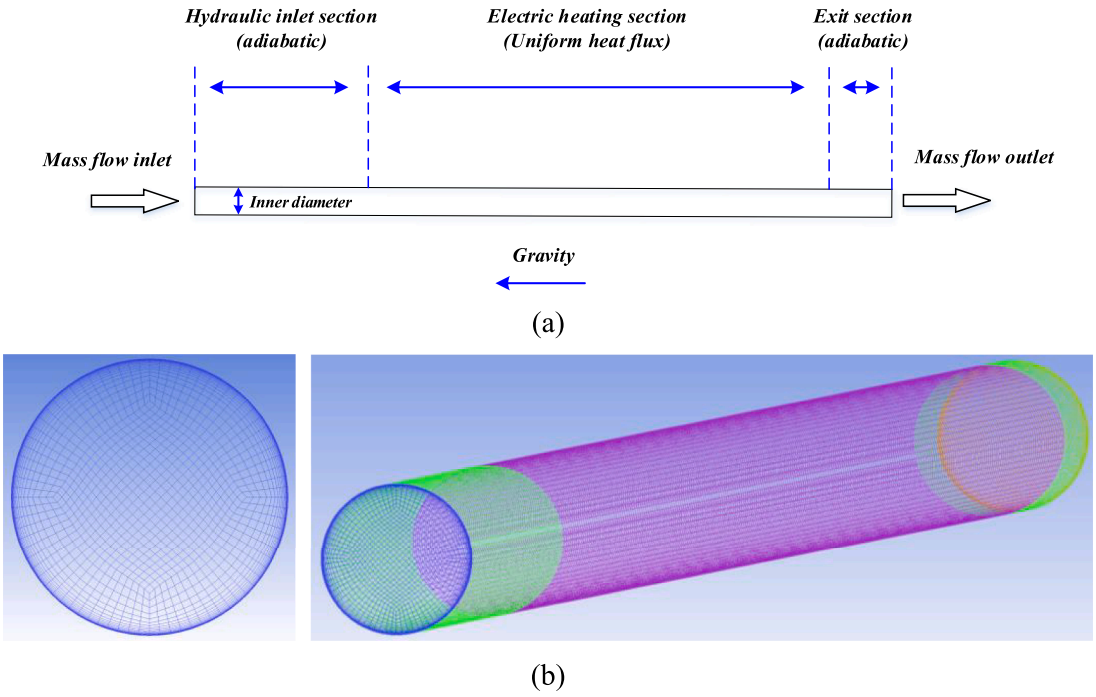

Fig. 3. (a) The physical model; (b) The generated mesh.

generally less than 0.65%. This occurrence can be attributed to the considerable long length of the tube, which effectively dilutes any influence caused by insufficiently developed turbulence at the inlet through averaging across its entire length. Moreover, during the actual experiments, there was a long hydraulic development section ($L/d \approx 50$) before the pressure drop test section, resulting in an inlet fluid flow that closely resembled fully developed turbulence. Therefore, setting the inlet turbulence intensity to correspond to fully developed turbulence is considered appropriate in the simulation of this study.

3.3. The selection of reference temperature

In our experiment, since each test condition corresponds to a single experimental point, it is necessary to determine the reference temperature of the fluid for each operating condition. It can be anticipated that, due to the relatively long length of the test section, there is a significant temperature difference between the inlet and outlet bulk fluids under the heating condition. Taking the arithmetic average of the inlet and outlet temperatures to define the reference temperature of whole tube section would introduce significant errors. Therefore, a similar verification method as in our previous work [47] was adopted to validate the method of defining the reference temperature. The specific process is described as *Supplementary Information Chapter 3*.

4. Result and discussion

In this section, the experimental and numerical results of the friction factors of sCO_2 are analyzed in detail. We also present the originassl data of frictional pressure drop and reference temperature obtained from experiments, as well as some analysis, which can be found in *Supplementary Information Chapter 4*. The experimental conditions are shown in Table 4.

4.1. Isothermal conditions

Fig. 6 illustrates the experimental results of friction factor of Tube A under isothermal conditions. As shown in Fig. 6(a), when the mass flow rate keeps unchanged, the friction factor exhibits a similar trend with *Re* under different pressures. It is worth noting that the friction factor follows an S-shaped bending trend with a decrease, followed by an increase, and then a decrease again as *Re* increases. The maximum value appears to be near pseudo-critical point. This is in stark contrast to the conventional theory of adiabatic flow resistance, where it is commonly accepted that an increase in *Re* leads to a decrease in the friction factor for single-phase fluids.

Some researchers have also reported the anomalous increase in friction factor near the pseudo-critical region[23, 48], but they did not provide a reasonable explanation. We re-examined and carefully analyzed the available experimental data on pressure drop in supercritical fluid flow from the existing literature [16,23,25,26,49,50]. Among them, the data from Dang et al. [49] were reprocessed, taking into account the acceleration pressure drop caused by density changes (based on the error bars provided in their article). The representative operating conditions are shown in Fig. 7, including the results from our own experiments. The positions of the pseudo-critical point are marked in line in each figure (when two data points are on either side of the pseudo-critical point, the middle value is used to represent the pseudo-critical point). Fig. 7(a) ~ (d) and (f) represent cooling conditions, while Fig. 7(e), (g) and (h) represent the adiabatic conditions.

As shown in Fig. 7(a) ~ (h), a careful comparison reveals a consistent anomalous increase in the friction factor near the pseudo-critical point. However, the locations of the maximum values vary, with some occurring before the pseudo-critical point, some after, and some precisely at the pseudo-critical point. Among these, the results of Dang et al. [49] (Fig. 7(a)), Jiang et al. [23] (Fig. 7(b)), and Gerimella et al. [50] (Fig. 7 (f)) indicate a peak value above the pseudo-critical point. Based on our analysis, it is more reasonable for the maximum value to occur above the pseudo-critical temperature under cooling conditions. In fact, according to the critical opalescence theory [51], near the critical point, the isothermal expansivity of the substance becomes significantly large, resulting in pronounced density fluctuations even with minor perturbations. Consequently, it can be inferred that near the critical point, the more remarkable density fluctuations would lead to additional momentum exchange between the fluid parcels and potentially resulting in a higher turbulent dissipation, which would most likely lead to a greater loss of frictional resistance. As the wall shear layer bears the main

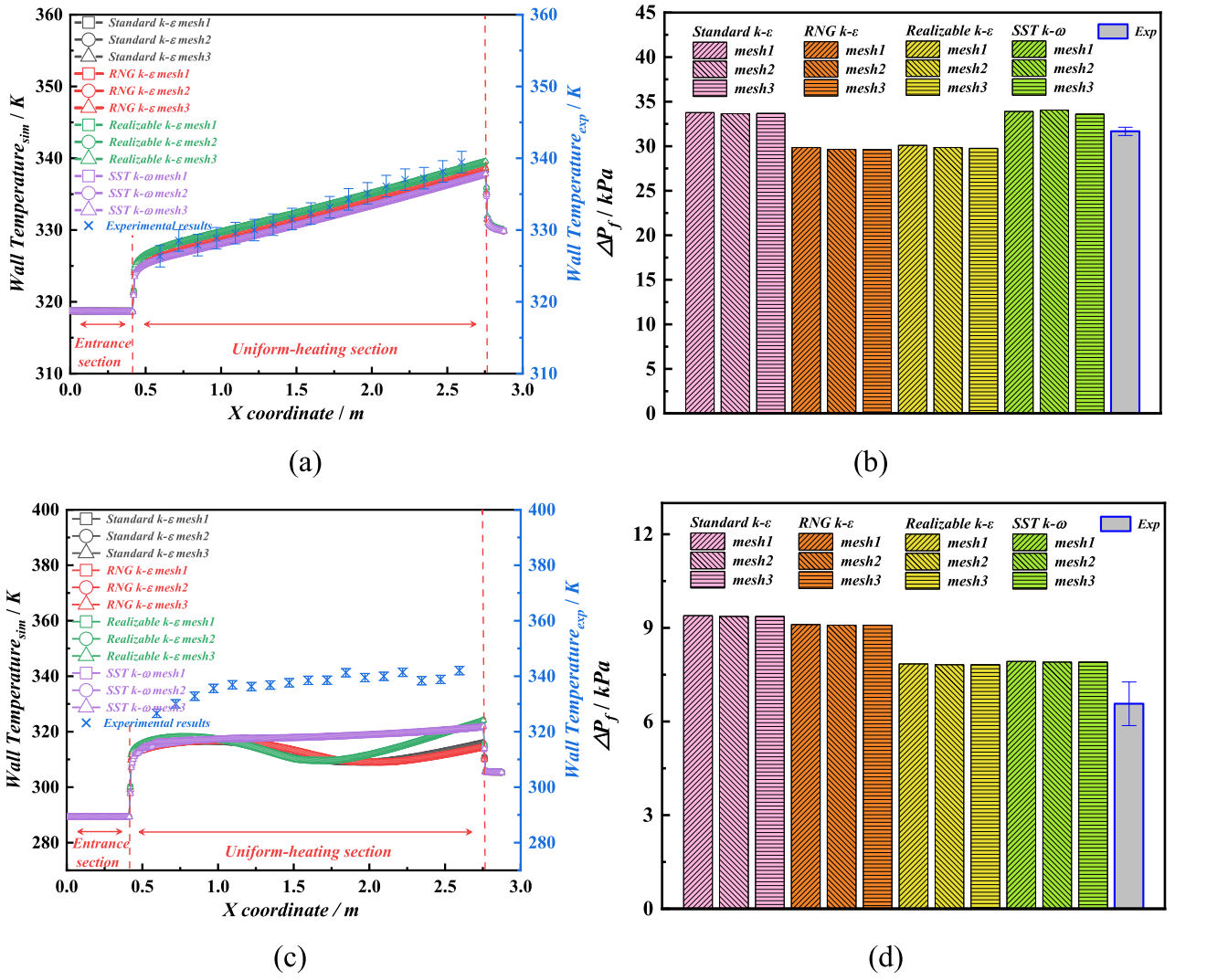

Fig. 4. Mesh independence check for different numerical models. (a) & (b): 7.6 MPa, 450 kg·h^{-1}, 45 kW·m^{-2}, 45.6 °C inlet (above T_{pc}); (c) & (d): 7.6 MPa, 450 kg·h^{-1},180 kW·m^{-2},16.1 °C inlet (below T_{pc}).

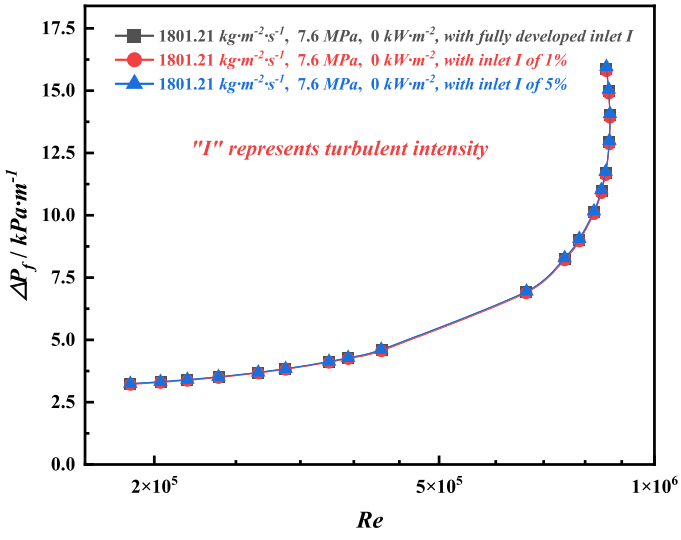

Fig. 5. The impact of inlet turbulence intensity on ΔP_f.

turbulent dissipation, under cooling conditions, when the wall

Table 4
The experimental conditions.

Tube A		Tube B	
Parameters	Range	Parameters	Range
Pressure / MPa	7.6 ~ 14	Pressure / MPa	7.6 ~ 14
The mass flow rate per unit area / kg·m^{-2}·s^{-1}	1200.81 ~ 3002.02	The mass flow rate per unit area / kg·m^{-2} ·s^{-1}	1104.56 ~ 2208.92
Reference temperature / °C	13 ~ 75	Reference temperature / °C	13 ~ 75
Wall heat flux / W·m^{-2}	0 ~ 180	Wall heat flux / W·m^{-2}	0 ~ 180

temperature is near the pseudo-critical point, the mainstream temperature is just higher than the pseudo-critical temperature. The fluid corresponds to the strongest turbulent dissipation at this time, i.e., it corresponds to the maximum friction factor. It is worth noting that the results from Andreson et al. [25] (Fig. 7(c)) and Zhao et al. [26] (Fig. 7 (d)) seem to contradict this pattern. We speculate that this discrepancy may be attributed to systematic errors caused by their experimental temperature measurement instruments or other factors. The results of Zhu et al. [48] (Fig. 7(g)) clearly demonstrate that the maximum friction factor occurs precisely at the pseudo-critical point for RP3 under adiabatic flow conditions. However, as shown in Fig. 7(h), in our experiment conducted at 7.6 MPa, the maximum friction factor is observed at a

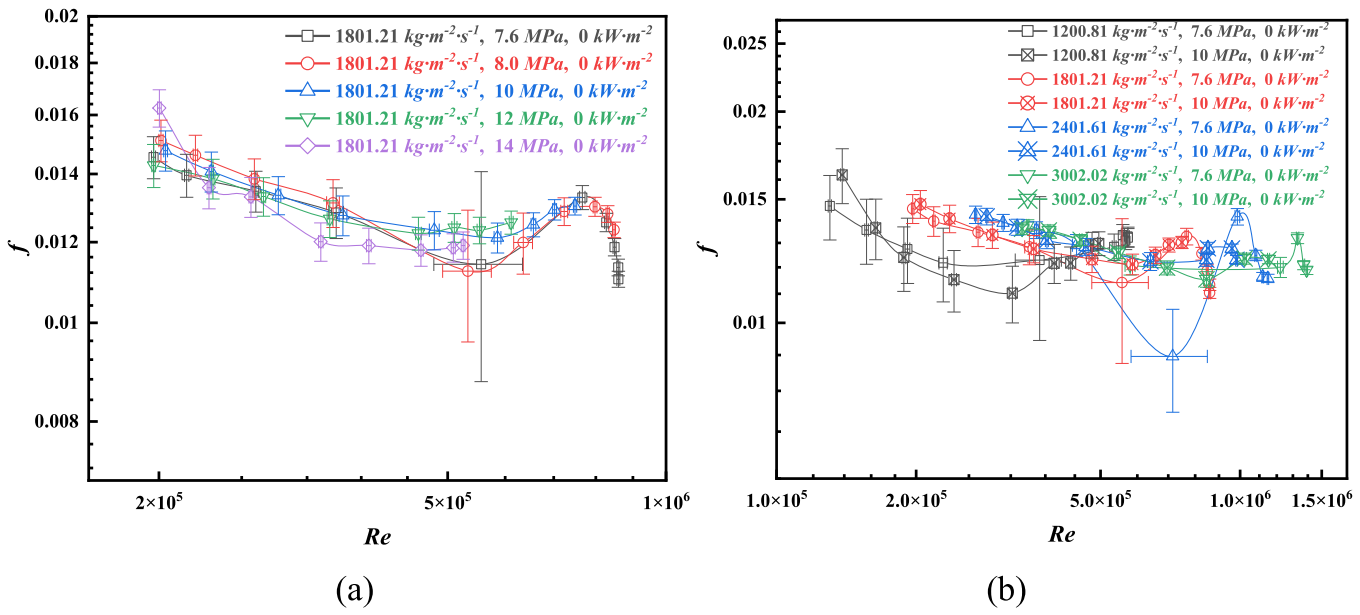

Fig. 6. The variation pattern of friction factor with *Re* for Tube A under experimental isothermal conditions: (a) Under different pressure; (b) Under different mass flow rate.

position higher than the pseudo-critical temperature. In fact, such a scenario is reasonable under the experimental conditions of our study. Due to significantly higher mass flow rate and tube diameter compared to most studies in the literature, heat dissipation within the tube becomes more significant. Even with a small degree of heat dissipation, the wall temperature would be slightly lower than the bulk fluid temperature, leading to a similar effect as observed under "cooling" conditions. Thus, the maximum friction factor obtained from our experiment exhibits a rightward shift. This also explains the phenomenon observed in Fig. S5(a) in *Supplementary Information*, where some experimental results at 8 MPa show slightly higher friction factors compared to the 7.6 MPa condition, indicating that the shear layer near these 8 MPa conditions still experiences higher density fluctuations compared to the 7.6 MPa condition.

Furthermore, as shown in Fig. 6(b), the variation trend of the friction factor with *Re* was compared for different mass flow rates in Tube A. This seemingly peculiar trend can be reasonably explained using the theory of critical density fluctuations. When the mass flow rate increases, the *Re* at which the pseudo-critical temperature is reached also increases. Therefore, the inflection points of the friction factor at higher mass flow rate shifts to a higher *Re*, which make the friction factor curves appear to exhibit an overall "rightward shift".

For Tube B, as shown in Fig. 8(a), the experimental friction factor under isothermal conditions exhibits a nearly constant trend both before and after the pseudo-critical point under different pressures. This is because, under the current *Re* and tube wall roughness, the flow is already in the "fully rough regime" [13], where the friction factor becomes independent of *Re*. However, what is interesting is that the friction factor seems to be situated on two distinct "plateau regions" below and above the pseudo-critical point. This phenomenon is more visually evident in Fig. 8(b). Under low mass flow rate (1104.56 $kg{\cdot}m^{-2}{\cdot}s^{-1}$), when *Re* reaches 5×10^5, the fluid bulk temperature has already crossed the pseudo-critical point and entered the "low plateau region". While under high mass flow rate (2208.92 $kg{\cdot}m^{-2}{\cdot}s^{-1}$), *Re* needs to reach 8×10^5 to transition the friction factor to the "low plateau region". This peculiar behavior may be attributed to the combined factors of high wall roughness, critical density fluctuation within the boundary layer, and nonlinear variations of thermophysical properties near the wall.

The friction factor results obtained from SST *k-ω* simulations for Tube A and Tube B (with an absolute roughness of 10 μm in simulation) under isothermal condition are shown in Fig. 9(a) ~ (b). As shown in Fig. 9(a), the simulated friction factor of Tube A exhibits a generally stable decreasing trend with increasing *Re* under different pressures. Meanwhile, the results in Fig. 9(b) indicate that in the rougher Tube B, the friction factor remains stable around a certain value and is not significantly affected by variations in *Re*. These results are consistent with the traditional theory of friction factor for single-phase fluids. However, the differences between the simulation and experimental values are evident: (1) In the isothermal case for Tube A, the simulation did not reproduce the anomalous increase in the friction factor near the pseudo-critical point. (2) In the isothermal case for Tube B, the friction factor did not exhibit two distinct "plateau regions" as observed in the experimental results. These discrepancies can be attributed to the inherent limitations of the RANS model itself. The RANS model, as a time-averaged filtering model for the Navier-Stokes equations, may inadequately account for the transient density fluctuation effects. Although it was verified in Section 3.2 that other RANS models may result in potential unphysical solutions, a comparison of the friction factor results obtained from different RANS models under the same operating conditions is still presented in Fig. 10 to further confirm the deficiencies of RANS models. As shown in Fig. 10, it is evident that none of the RANS models can accurately capture the near pseudo-critical anomaly in the friction factor observed in the experimental results. The differences among the four RANS models only exist in the baseline levels of the friction factor. Further research is imperative to enhance the existing RANS model and extend its applicability to scenarios involving significant density fluctuations.

4.2. Non-isothermal conditions

Fig. 11(a) ~ (c) present the experimental results of friction factor of Tube A under different heat flux conditions. Generally, as *Re* increases, there is an overall downward trend in the friction factor. The comparison between Fig. 11(a) and Fig. 11(b) shows that when the ratio of heat flux to mass flow rate is relatively small, the influence of heat flux on the friction factor is weakened. Moreover, by comparing Fig. 11(a) and Fig. 11(c), it can be observed that under conditions approaching the critical pressure, the effect of heat flux on the friction factor is suppressed compared to conditions far from the critical pressure.

The experimental results of Tube B under different heat flux are

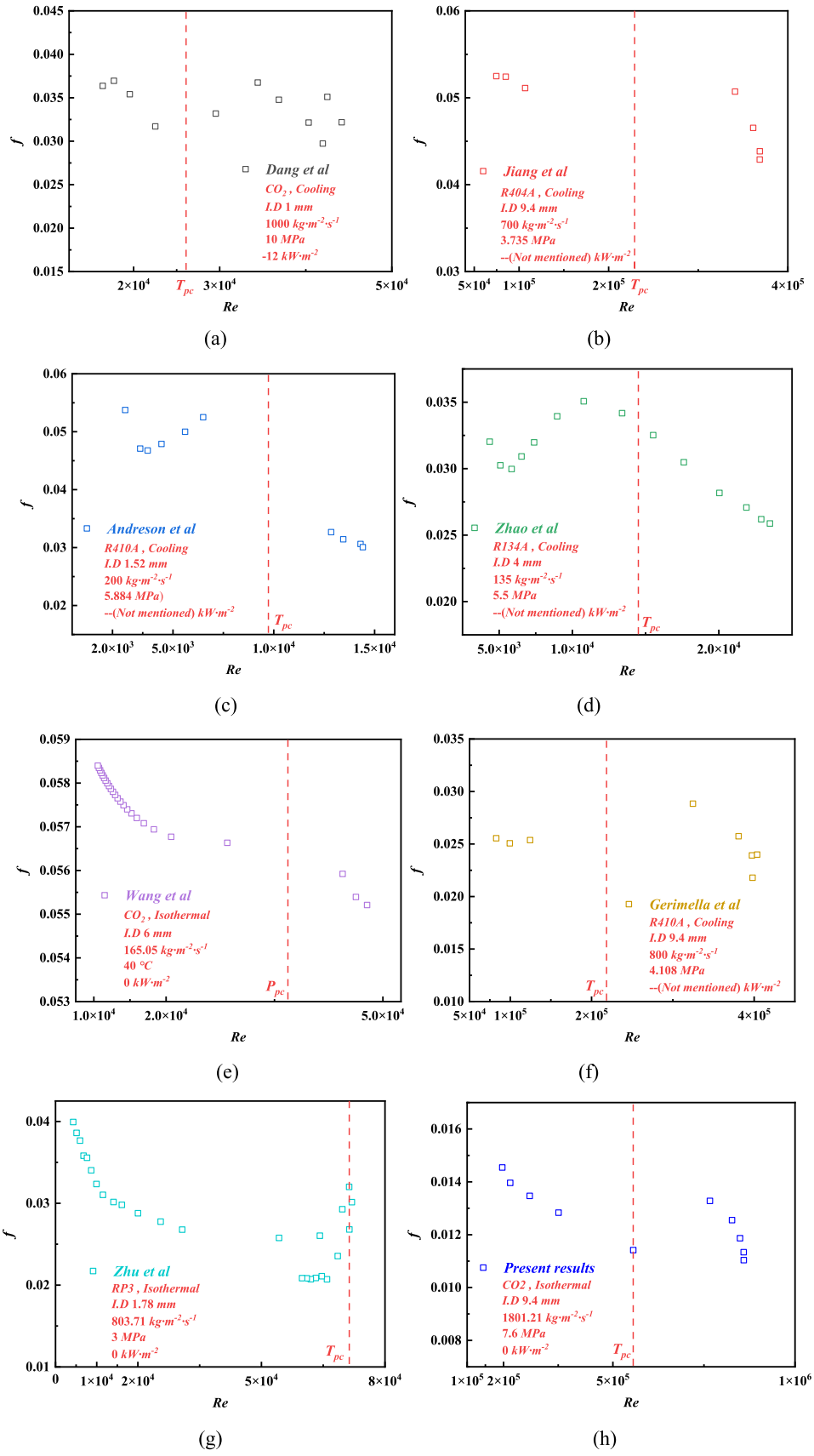

Fig. 7. The variation pattern of friction factor with *Re* from different researchers: (a)Dang et al. [49]; (b)Jiang et al. [23]; (c)Andreson et al. [25]; (d)Zhao et al. [26]; (e)Wang et al. [16]; (f)Gerimella et al. [50]; (g);Zhu et al. [48]; (h)Present results.

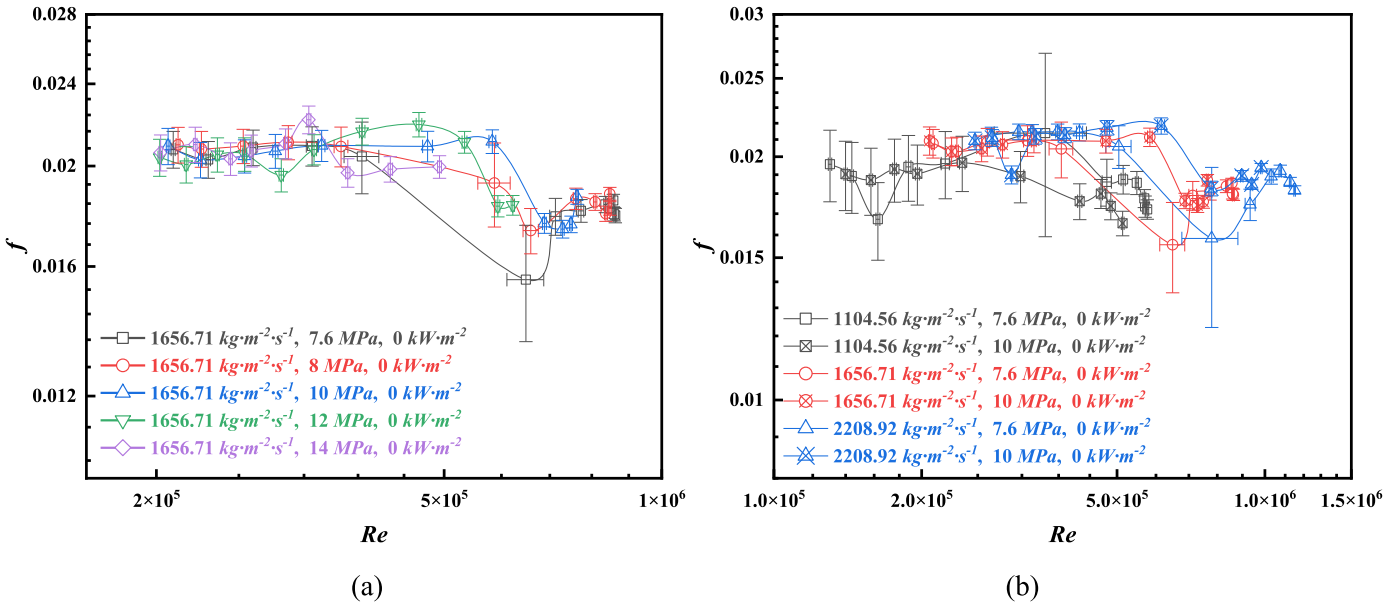

Fig. 8. The variation pattern of friction factor with *Re* for Tube B under experimental isothermal conditions: (a) Under different pressure; (b) Under different mass flow rate.

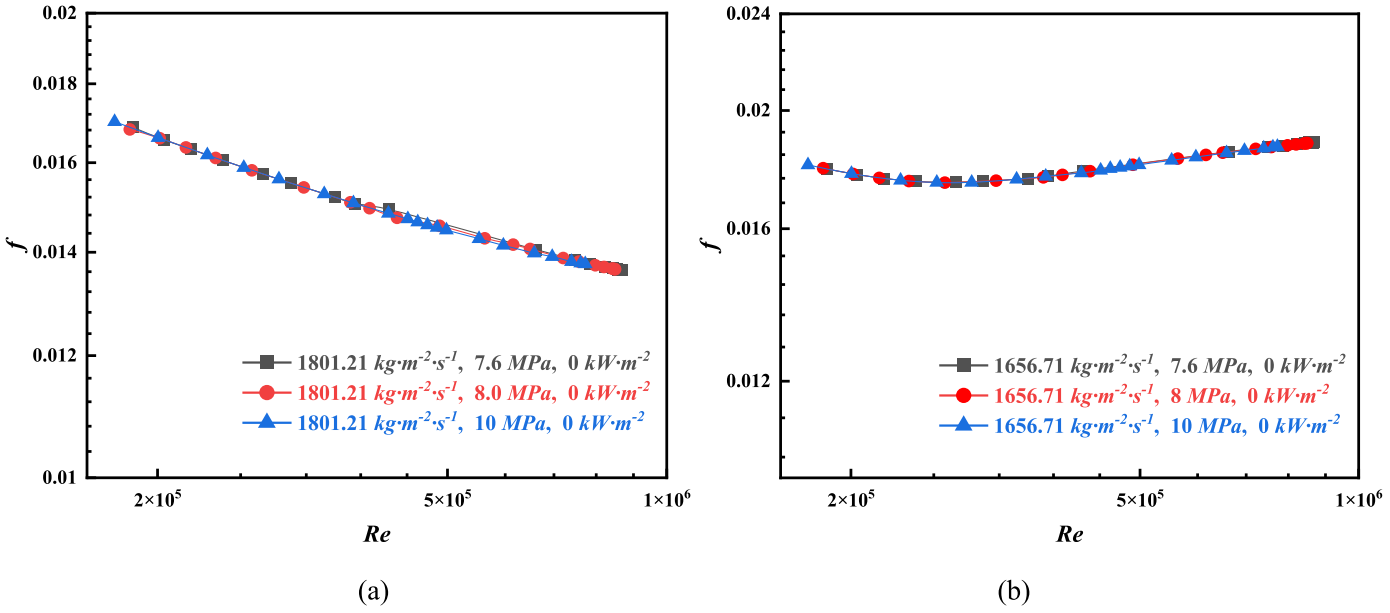

Fig. 9. The variation pattern of friction factor with *Re* under simulated isothermal conditions using the SST *k-ω* model: (a) Tube A; (b) Tube B (Roughness height was set to 10 μm).

presented in Fig. 12(a) ~ (c). Under non-isothermal conditions, the variation pattern of the friction factor in rough tubes remains slightly complex mainly due to its characteristic of being distributed at "different plateau regions " on both sides of the critical point, as mentioned earlier. However, a straightforward comparison between the results of Fig. 12 and Fig. 11 would reveal that the influence of heat flux on the friction factor in rough tubes is somewhat suppressed by the effect of high wall roughness. Due to the limited information provided by experimental results, a more profound understanding requires assistance from simulation tools.

Although the RANS model failed to predict the anomalous increase in the friction factor near the pseudo-critical temperature, it still provides relatively accurate trends for friction factor variation under heating conditions. As shown in Fig. 13(a), the simulated trend of the friction factor with *Re* for Tube A exhibits a similar pattern to the experimental results in Fig. 11(a) under different heat flux conditions. In Fig. 13(b), the simulated friction factor of the rougher tube shows a relatively less pronounced decreasing trend with increasing heat flux compared to Tube A (Fig. 13(a)), which is similar to the experimental results shown in Fig. 12. Therefore, we can still utilize the RANS model to discuss certain phenomena occurring within the flow field and obtain valuable results. Considering that turbulent viscous stress contributing only a minimal fraction to the overall mechanical energy dissipation [34], in this study, we focus solely on analyzing the volume-averaged Reynolds stress within the flow field to assess the influence of wall roughness. Fig. 14 presents a comparison of the relationship between Reynolds stress and *Re* for Tube A and Tube B at 7.6 MPa. It is observed that, under the same *Re*, the Reynolds stress of the rougher tube is less affected by

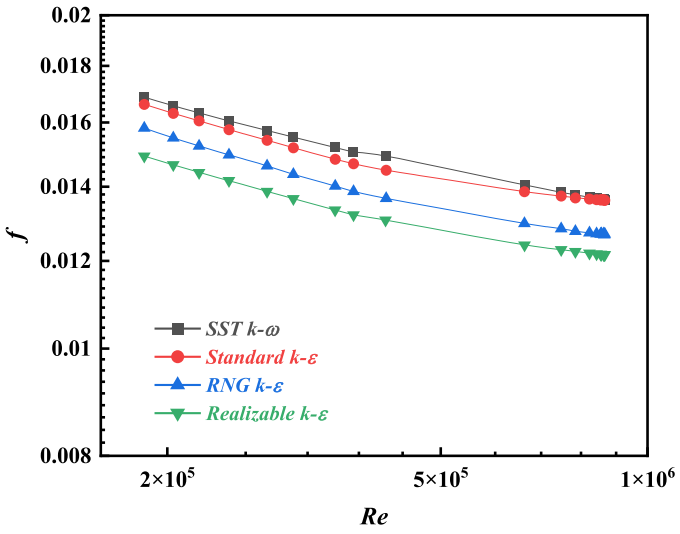

Fig. 10. The variation trend of friction factor with *Re* obtained from different RANS models under the operating conditions of 7.6 MPa, 1801 kg·m^{-2}·s^{-1}, 0 kW·m^{-2}.

the heat flux. This implies that the friction factor of the rougher tube exhibits reduced sensitivity to changes in heat flux, which is consistent with the experimental results.

Furthermore, as shown in Fig. 15(a), (b), (e), (f), the simulation results for the distribution of Reynolds stress (only absolute values are shown) and turbulent velocity fluctuations with respect to wall distance under conditions above and below the pseudo-critical point further indicate that within the fluid domain, the influence of heat flux on Reynolds stress is significantly limited in rougher tubes. In contrast, in smoother tubes, Reynolds stress decreases significantly with increasing heat flux. As presented in Fig. 15(c), (d), (g), (h), the trend in Reynolds stress variation is found to be strongly connected with the level of turbulent velocity fluctuations. It can be deduced that with the enhancement of wall roughness effects, there is a weakened correlation between the level of turbulent mean velocity fluctuations and thermal boundary conditions. Consequently, the friction factor in rough tubes is less affected by heat flux compared to smooth tubes.

4.3. New friction factor correlations for variable property fluids based on the law-of-the-wall

As early as the 1930s, Prandtl obtained an analytical solution for the friction factor of a smooth tube by integrating the logarithmic velocity law along the radial direction of the tube [15]. According to Prandtl's calculation, if a logarithmic velocity law exists near the wall as Eq. (4):

$$u^+ = \frac{1}{\kappa} lg(y^+) + B \tag{4}$$

Where u^+ is the dimensionless velocity; y^+ is the dimensionless wall-normal distance; κ and B are constants. The analytical solution for the friction factor of smooth tube can be expressed in the form of Eq. (5).

$$f = \left[a\lg\left(Re\sqrt{f}\right) + b\right]^{-2} \tag{5}$$

This relationship is derived for fluids under constant property conditions. However, for variable property fluids, the drastic variations in the thermophysical properties lead to significant differences in the statistical characteristics of various parameters within the turbulent flow field. This implies that the conventional velocity scaling law cannot yield a logarithmic velocity distribution. It is worth noting that Ma et al. [52] verified, through direct numerical simulation (DNS) simulations, that the velocity law of variable property fluids can satisfy the logarithmic distribution by employing the Van Driest transformation. It means that after transforming $u^+_{VD} = \int_0^{u^+} \sqrt{\left(\frac{\rho}{\rho_w}\right)} du^+$, we can obtain the logarithmic velocity law as Eq. (6) below.

$$u^+_{VD} = \frac{1}{\kappa}\ln(y^+) + B \tag{6}$$

Building upon this, we endeavor here to derive the friction factor for a variable property fluid.

Considering the flow of a variable property fluid in a circular tube, we can derive the following equation based on the principle of force balance:

$$\tau_w \cdot 2\pi R \cdot L = \Delta P_f \cdot \pi R^2 \tag{7}$$

Where τ_w is the wall shear stress; R is the radius of the tube; L is the length of the tube; and ΔP_f is the frictional pressure drop. The definition of wall shear stress is given by Eq. (8).

$$\tau_w = u_\tau^2 \rho_w \tag{8}$$

Where u_τ is the wall shear velocity and ρ_w is the fluid density at the wall.

Furthermore, according to the definition of the friction factor, we have:

$$\Delta P_f = f \cdot \frac{L}{d} \cdot \frac{\rho_b u_b^2}{2} \tag{9}$$

Where ρ_b is the bulk fluid density; u_b is the bulk fluid velocity. By combining Eq. (7) ~ (9), we can obtain Eq. (10).

$$f = 8\frac{u_\tau^2}{u_b^2}\frac{\rho_w}{\rho_b} \tag{10}$$

Furthermore, the non-dimensional wall distance for variable property fluid can be represented as Eq. (11).

$$y^+ = \frac{y u_\tau \rho_w}{\mu_w} \tag{11}$$

Where y represents the wall-normal distance.

Combining Van Driest transformation and Eq. (11), we can get Eq. (12):

$$\int_0^{u^+} \sqrt{\left(\frac{\rho}{\rho_w}\right)} du^+ = \frac{1}{\kappa} ln\left(\frac{y u_\tau \rho_w}{\mu_w}\right) + B \tag{12}$$

For the left-hand side of Eq. (12), in order to obtain a solution for the integral, it is necessary to know the specific analytical expression of ρ as a function of u^+ (i.e., u/u_τ). However, under the current conditions, obtaining such an expression is nearly impossible. Therefore, for simplification purposes, we assume the existence of a reference density ρ_r, such that the integral result could satisfies the relationship given by Eq. (13) as follows.

$$\int_0^{u^+=u_b^+} \sqrt{\left(\frac{\rho}{\rho_w}\right)} du^+ \approx \left(\frac{\rho_r}{\rho_w}\right)^A \int_0^{u^+=u_b^+} du^+ = \left(\frac{\rho_r}{\rho_w}\right)^A \frac{u_b}{u_\tau} = \left(\frac{\rho_r}{\rho_w}\right)^A \cdot \frac{2\sqrt{2}}{\sqrt{f}} \cdot \sqrt{\frac{\rho_w}{\rho_b}} \tag{13}$$

The derivation of Eq. (13) utilizes the relationship expressed in Eq. (10), and A is an undetermined constant. Considering the approximation of Eq. (13) and its physical meaning, ρ_r is expected to fall within the range of ρ_w and ρ_b. For ease of understanding, we denote it as ρ_f.

By combining the right-hand side of Eq. (12) with Eq. (10), the Eq. (14) can be obtained:

$$\begin{aligned} &\frac{1}{\kappa} ln\left(\frac{y u_\tau \rho_w}{\mu_w}\right) + B = \frac{1}{\kappa} ln\left(\frac{y}{d} \cdot \frac{d u_b \rho_b}{\mu_w} \cdot \frac{u_\tau \rho_w}{u_b \rho_b}\right) + B \\ &= \frac{1}{\kappa} ln\left(\mathrm{Re_w}\sqrt{f}\sqrt{\frac{\rho_w}{\rho_b}}\right) + \frac{1}{\kappa} ln\left(\frac{y}{2\sqrt{2}d}\right) + B \end{aligned} \tag{14}$$

In this case, due to the assumption in Eq. (13) that the u^+ on left-hand

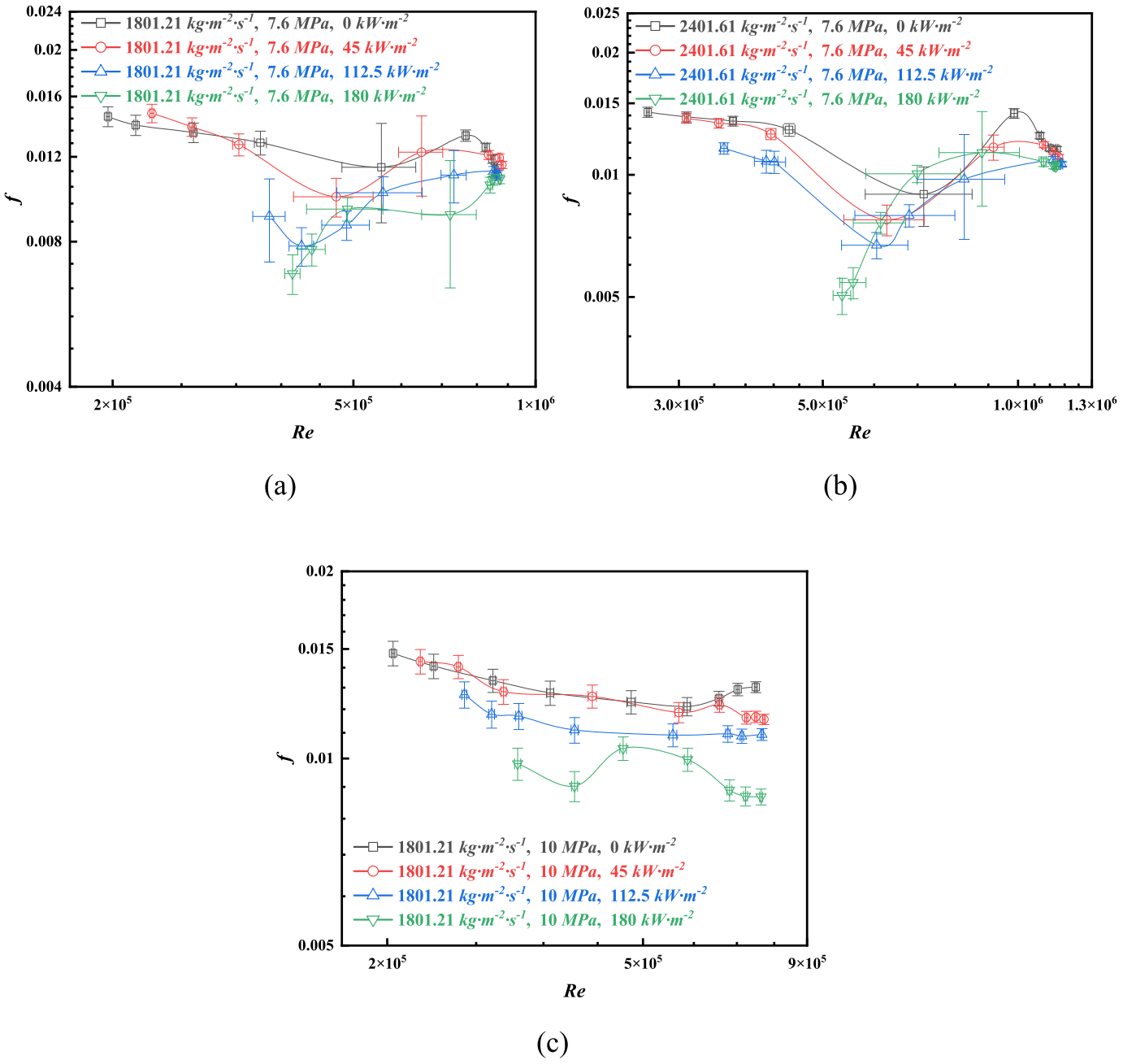

Fig. 11. The variation pattern of friction factor with *Re* for Tube A under experimental non-isothermal conditions: (a) Under near critical pressure (7.6 MPa) and a lower mass flow rate; (b) Under near critical pressure (7.6 MPa) and a higher mass flow rate; (c) Under far beyond critical pressure (10 MPa).

side of Eq. (12) takes the value of u_b^+ ($u_b^+ = u_b/u_\tau < u_{axis}/u_\tau$, where u_{axis} is the axial velocity), the y on right-hand side of Eq. (14) should be less than $d/2$. Considering the physical interpretation of turbulent flow inside the tube, the thickness of the fluid boundary layer undergoes varying degrees of compression as *Re* changes. Therefore, y should also be a variable that varies with *Re*. In this study, we assume $\frac{1}{\kappa} ln\left(\frac{y}{2\sqrt{2}d}\right) = \frac{C}{\mathrm{Re}_{wf}}$ (where C is an undetermined constant and should be a negative value). Furthermore, by converting the natural logarithm to a logarithm with base 10 and combining Eq. (13) and Eq. (14), Eq. (15) can be obtained.

$$f = \left(\frac{\left(\frac{\rho_f}{\rho_w}\right)^A \sqrt{\frac{\rho_w}{\rho_b}}}{\frac{1}{\kappa \cdot 2\sqrt{2} \cdot \lg(e)} \cdot \lg\left(\mathrm{Re}_w \sqrt{f} \sqrt{\frac{\rho_w}{\rho_b}}\right) + B + \frac{C}{\mathrm{Re}_{wf}}} \right)^2 \tag{15}$$

Eq. (15) differs significantly from Prandtl's correlation (Eq. (5)) in that the friction coefficient is no longer determined by the *Re* of the bulk fluid (i.e., Re_b), but by the *Re* at the wall (i.e., Re_w). This also explains why Allen [17]obtained a friction factor for water under heating conditions that aligns better with experimental values when replacing Re_b in the Blasius correlation with Re_w (it should be noted that at low pressures, water's viscosity is significantly influenced by temperature while density remains almost constant). In the case of non-isothermal sCO_2, the significant temperature gradient between the bulk fluid and the wall surface, combined with the substantial impact of temperature on

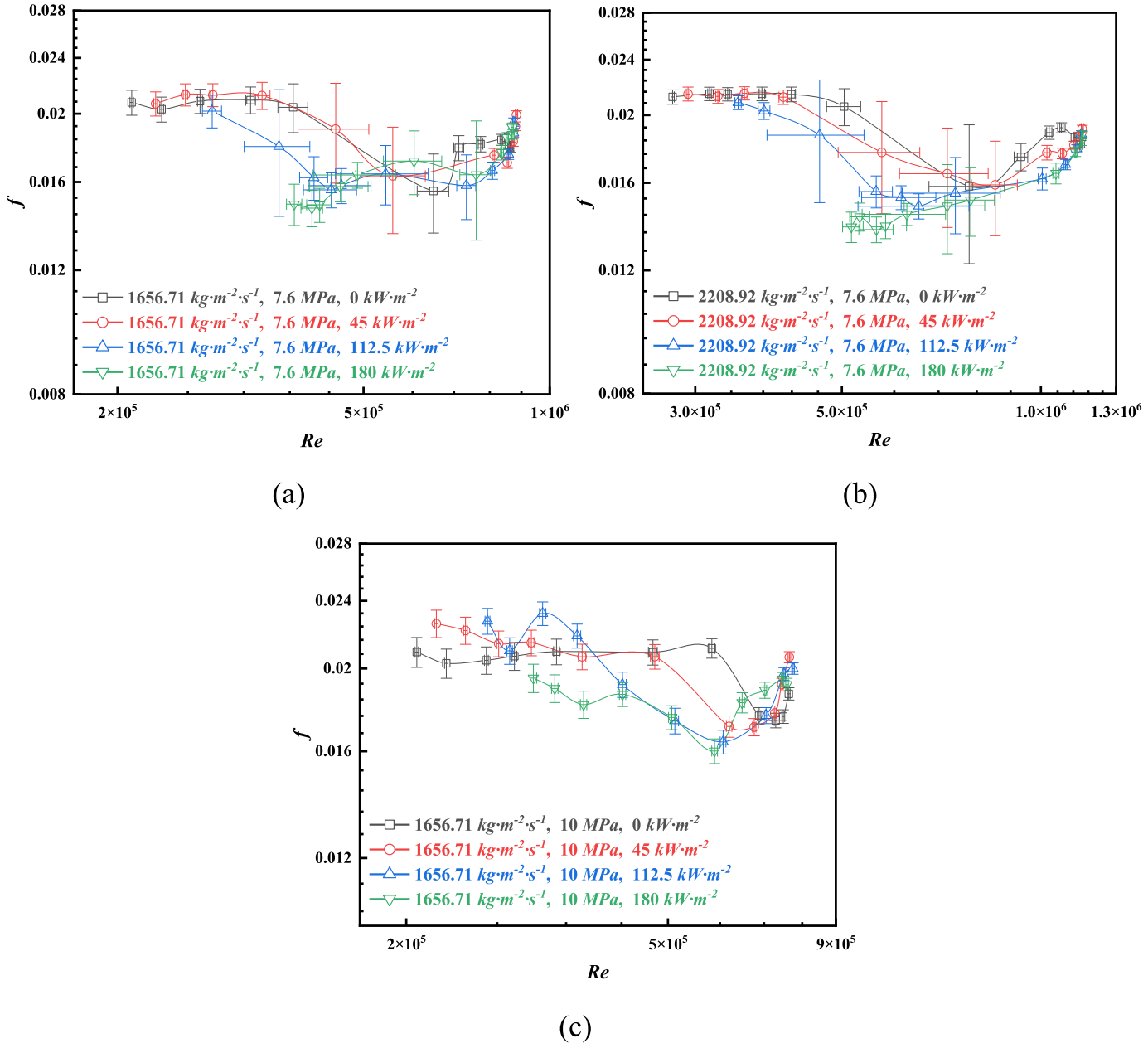

Fig. 12. The variation pattern of friction factor with *Re* for Tube B under experimental non-isothermal conditions: (a) Under near critical pressure (7.6 MPa) and a lower mass flow rate; (b) Under near critical pressure (7.6 MPa) and a higher mass flow rate; (c) Under far beyond critical pressure (10 MPa).

density, further complicates the influence of heat flux on the friction factor. This effect is primarily reflected in the numerator of Eq. (15), where the density gradient between the wall surface and the bulk fluid becomes larger as the heat flux increases.

Ma et al. [52] validated the rationality of setting κ=0.41 for variable property fluid. Therefore, in this study, we adopt $\frac{1}{0.41\cdot 2\sqrt{2}\cdot\lg(e)} = 1.9856$. In the case of rough walls, the roughness effect primarily alters the constant B in the logarithmic law [53]. Through extensive attempt, we defined the roughness effect using the relationship described by Eq. (16).

$$f = \left(\frac{\left(\frac{\rho_L}{\rho_w}\right)^A \sqrt{\frac{\rho_w}{\rho_b}}}{1.9856\cdot\log\left(\mathrm{Re}_w\sqrt{f}\sqrt{\frac{\rho_w}{\rho_b}}\right) + B + \frac{C}{\mathrm{Re}_w f} + D\cdot\log\left(\frac{\left(\mathrm{E}+\frac{\varepsilon}{d}\mathrm{Re}_w f\right)^F}{\mathrm{Re}_w\sqrt{\frac{\rho_w}{\rho_b}}}\right)} \right)^2 \tag{16}$$

Where ε/d is the relative roughness; A, B, C, D, E, and F are undetermined coefficients. ρ_f is defined as the harmonic mean density, given by $\frac{2\rho_b\rho_w}{\rho_b+\rho_w}$.

To accurately determine the coefficients in Eq. (16), a regression analysis was conducted using an extended database. The database includes various experimental data points, including 381 data points from our own experiments, 29 data points from Yamashita et al. [22] for R22 heating flow, 65 data points from Dang et al. [49] for CO_2 cooling flow,

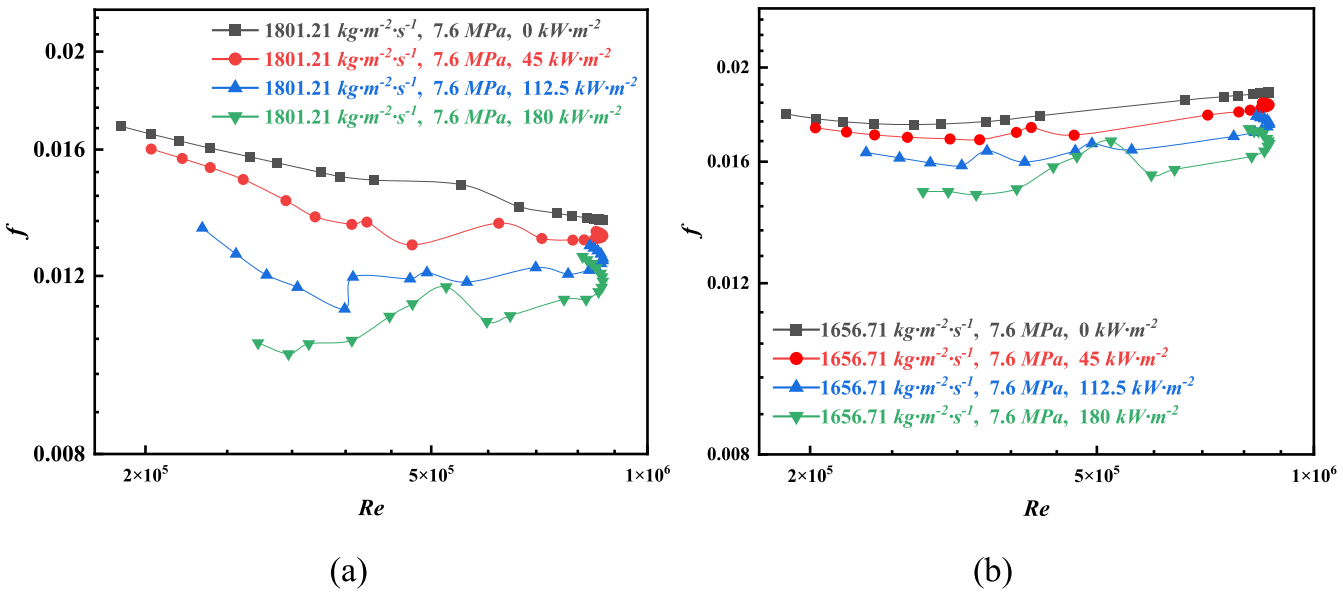

Fig. 13. The relationship between friction factor and *Re* from SST *k-ω* simulations (a) Tube A, at 7.6 MPa; (b) Tube B (Roughness height was set to 10 μm), at 7.6 MPa.

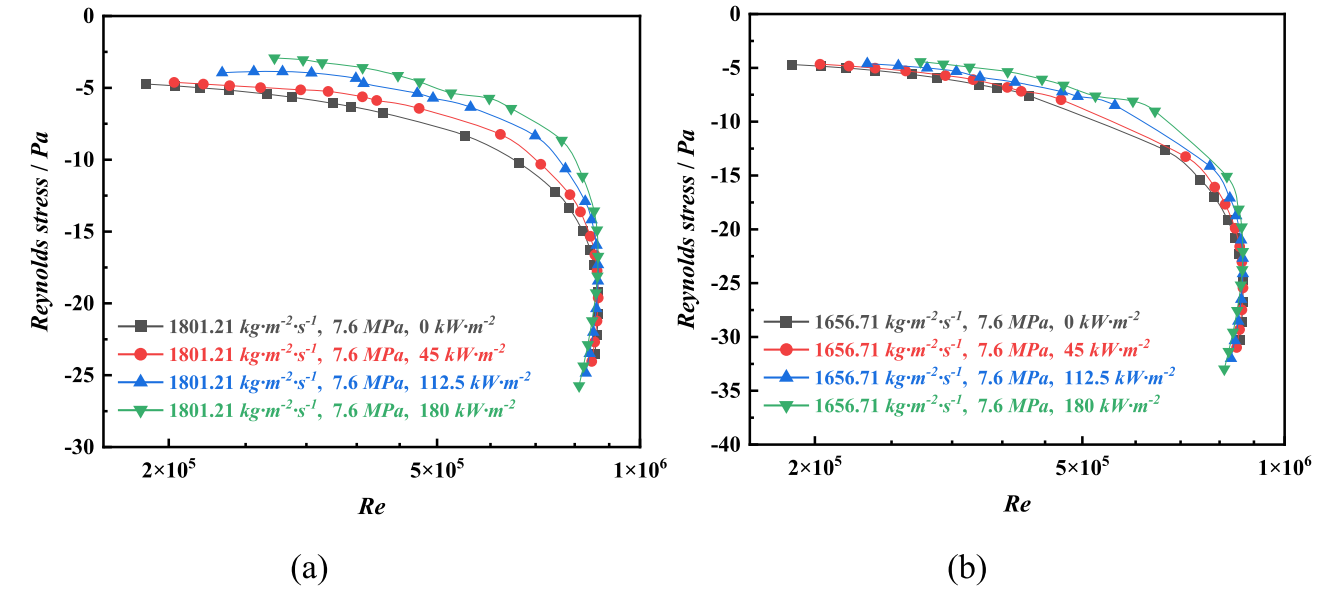

Fig. 14. The relationship between Reynolds stress and *Re* from SST *k-ω* simulations under non-isothermal conditions: (a) Tube A, at 7.6 MPa; (b) Tube B, at 7.6 MPa.

193 data points from Zhang et al. [28] for RP3 adiabatic flow, 215 data points from Zhu et al. [48] for RP3 adiabatic flow, 246 data points from Wang et al. [16] for CO_2 adiabatic flow. The roughness of the experimental tubes in the studies by Yamashita and Dang was not explicitly mentioned. Based on our experience, the absolute roughness of their tubes was assumed to be 1.5 μm. Besides, data points with $Re < 3000$ were excluded from regression. It is worth noting that the experimental conditions of Zhu et al. [48] are similar to those of Zhang et al. [28], but their results for RP3 above the pseudo-critical point show large discrepancies. After careful comparison and consideration, the experimental data from Zhang et al. above the pseudo-critical point were excluded.

The Sequential Quadratic Programming (SQP) algorithm, available in the Statistical Package for the Social Sciences (SPSS) software, was used to estimate the coefficients in Eq. (16). The obtained results are presented in Table 5 below. The coefficient of determination (R^2) was found to be 0.990, indicating a well fit of the correlation.

We selected relatively newly proposed correlations for comparison, including those proposed by Wang et al. [16], Fang et al. [29], Zhang et al. [30], Zhu et al. [34], and Hao et al. [32]. The expressions proposed by these authors are given here as Eq. (17) ~ (21).

Wang et al. (2014):

$$\frac{1}{\sqrt{f}} = -2.34\cdot\lg\left(\frac{\varepsilon}{1.72d} - \frac{9.26}{\mathrm{Re}}\cdot\lg\left(\left(\frac{\varepsilon}{29.36d}\right)^{0.95} + \left(\frac{18.35}{\mathrm{Re}}\right)^{1.108}\right)\right) \tag{17}$$

Fang et al. (2020):

$$f = 0.0127\left(\ln\left(650\left(\frac{\varepsilon}{d}\right)^{0.67} + \left(\frac{99000}{\mathrm{Re}}\right)^{1.32} + 0.066Ch\right)\right) \tag{18}$$

Zhang et al. (2021):

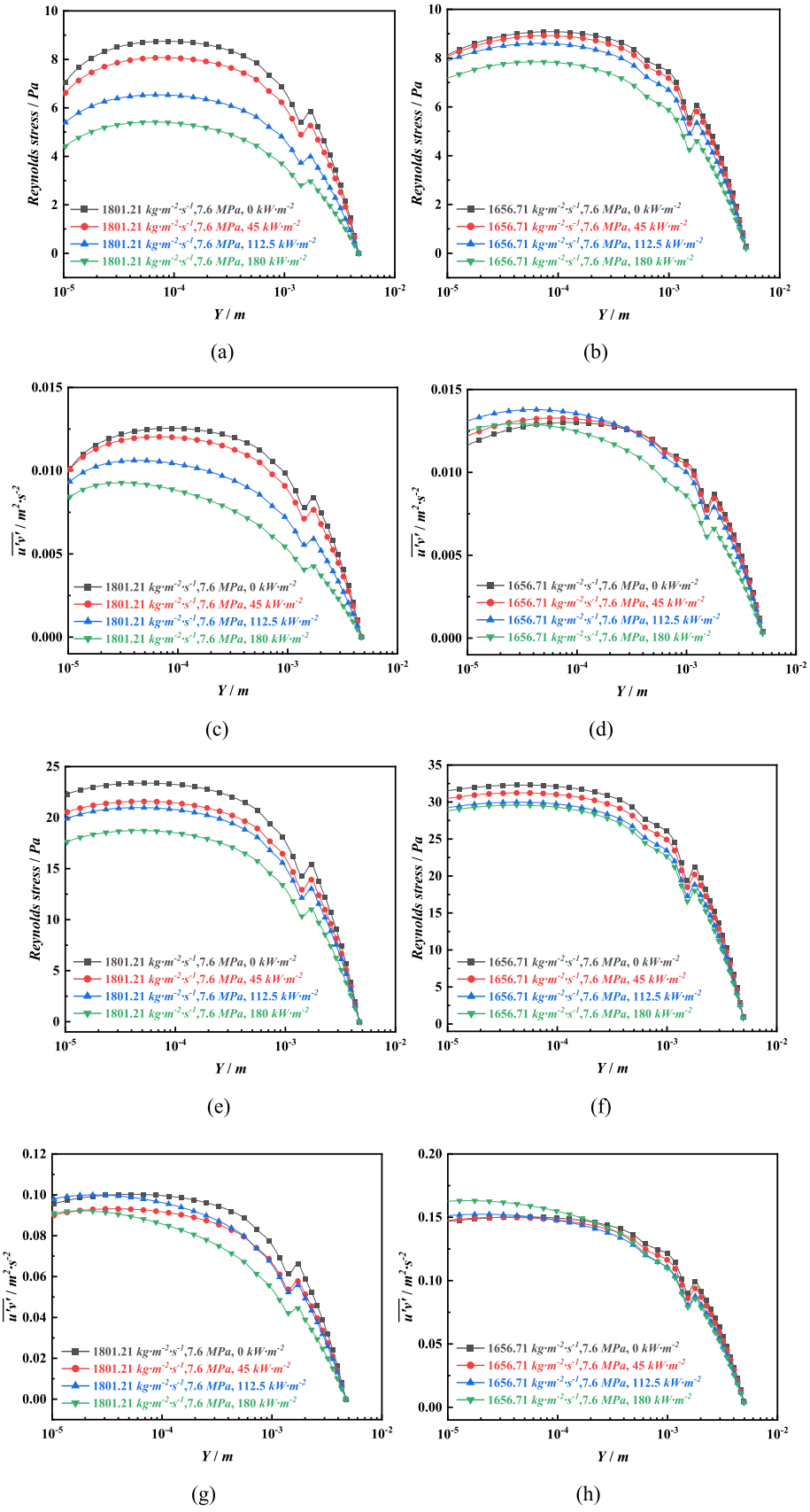

Fig. 15. The relationship between Reynolds stress and turbulent velocity fluctuations with respect to wall distance from SST k-ω simulations: (a) & (c): Tube A at reference bulk temperature of 29.5 ± 0.5 °C (Below T_{pc}); (b) & (d): Tube B at reference bulk temperature of 29.4 ± 0.6 °C (Below T_{pc}); (e) & (g): Tube A at reference bulk temperature of 40.7 ± 1 °C (Above T_{pc}); (f) & (h): Tube B at reference bulk temperature of 40.7 ± 1 °C (Above T_{pc}).

Table 5
The estimated results of the undetermined coefficients.

Coefficient	Estimated result (range of 95% confidence interval)
A	0.8770 (0.8300 ~ 0.9209)
B	1.8959 (1.7837 ~ 2.0253)
C	-31.0299 (-42.3189 ~ -19.2432)
D	3.5981 (3.5676 ~ 3.6250)
E	1.8495 (1.6388 ~ 2.0799)
F	0.3963 (0.3806 ~ 0.4082)

$$f = \frac{2.15K^{0.027}}{\mathrm{Re}^{0.342}} \tag{19}$$

Zhu et al. (2022):

$$f = \frac{1}{(1.82\cdot\lg(\mathrm{Re}) - 1.64)^2}\cdot\left(\frac{\rho_w}{\rho_b}\right)^{1.185(1+Xi)^{-0.204}}\left(\frac{\mu_w}{\mu_b}\right)^{-4.170(1+Xi)^{-1.692}} \tag{20}$$

Hao et al. (2023):

$$f = \frac{1.1228\chi^{0.1078}}{\mathrm{Re}^{0.287}} \tag{21}$$

The results for difference correlation are shown in Fig. 16. Among all the correlations in the literature, Wang's correlation exhibits relatively good performance, with 88% of the data points fall within ±20% absolute deviation range. However, as indicated in Fig. 16(a), the results for Tube A, Tube B, and Yamashita show a trend of "horizontal distribution", indicating that Wang's correlation significantly overestimates the friction factor when predicting heating conditions. In Fig. 16(b), Fang's results generally underestimated the results of heating condition. In Fig. 16(c), Zhang's correlation also shows significant deviations, and when the wall heat flux is zero (i.e., adiabatic flow), the calculation results of this correlation will lead to singular values ($f = 0$). In Fig. 16 (d), Zhu's correlation performs relatively well in predicting the friction factor for low roughness tubes, but since the correlation does not include the roughness effect, it produces significantly higher estimates for Tube B and the case of Wang et al. In Fig. 16(e), Hao's correlation generally overestimates the friction coefficient, possibly due to the fact that it was derived from experimental results for horizontal tube. The results of our proposed correlation demonstrate good prediction accuracy for both low and high roughness, heating and cooling processes, as well as subcritical and supercritical conditions. The average absolute error (MAE) of the predictions is 7.11%, which represents a decrease of 24.7% compared to the current best results (9.44%). The root mean square error (RMSE) is 10.83%, showing a decrease of 32.4% compared to the current best results (16.02%). Furthermore, 94% of the data points fall within the ±20% absolute deviation range, indicating an improvement of 6-percentage points compared to the current best results (88%).

Although the results are promising, there is still room for further improvement. This is because the correlation proposed in our article does not incorporate dimensionless numbers related to critical density fluctuations effects. In future research, it is necessary to combine DNS with high-pressure flow measurement techniques, which will contribute to a deeper understanding of fluid flow dynamics of supercritical fluids.

To further validate the universality of the correlation proposed in our article, we compared it with the Filonenko [35] correlation, which is widely recognized as an correlation capable of accurately predicting friction factors in smooth tubes. By substituting $\varepsilon/d = 0$ and considering constant properties, the friction factor correlation degrades to Eq. (22).

$$f = \left(\frac{1}{1.9856\cdot\log(\mathrm{Re}\sqrt{f}) + 1.8959 - \frac{31.0299}{\mathrm{Re}f} + 3.5981\cdot\log\left(\frac{(1.8495)^{0.3963}}{\mathrm{Re}}\right)}\right)^2 \tag{22}$$

The comparison between Eq. (22) and the Filonenko correlation in the Re range of $10^4 \sim 10^8$ are shown in Fig. 17. The results indicate that the maximum error is approximately 5% at Re of 10^4. When $Re > 10^5$, the difference between the two becomes negligible, suggesting that the correlation proposed in this paper can be well extrapolated to smooth tubes.

It is worth mentioning that although the friction factor correlation proposed here is an implicit function, it does not require solving the implicit equation itself. A simple and feasible computational method involves initially estimating the friction factor using the Blasius correlation [12] ($f = 0.3164\cdot Re^{-0.25}$) and then substituting the result into the correlation, which yields an initial solution. The initial solution can be further substituted into the correlation iteratively until a satisfactory convergence is achieved. Through extensive testing, it has been found that the correlation converges very quickly, typically within 2 ~ 3 iterations, to obtain the converged result.

5. Conclusion

In summary, this paper combines experimental, numerical, and theoretical studies to investigate the isothermal and non-isothermal flow resistance characteristics of sCO_2 in tubes with different surface roughness. The main conclusions obtained are as follows:

(1) According to the experimental results, for supercritical fluids with variable properties, the friction factor decreases with increasing heat flux under heated boundary conditions. In addition, in pipes with low surface roughness, the effect of heat flux on the friction factor is more significant than in pipes with high surface roughness.
(2) RANS simulation can qualitatively reflect the degree to which supercritical fluids with variable properties are affected by heat flux in tubes with different surface roughness. The reason why the friction factor in tubes with high surface roughness is less affected by heat flux is attributed to the weakening of the influence of heat flux on the average velocity fluctuations.
(3) The experimental results demonstrate a significant increase in the friction factor of sCO_2 near the pseudo-critical point. We firstly used the density fluctuation theory to explain this anomaly: it is probably caused by the additional momentum exchange between fluid parcels due to the abnormally high density-fluctuations of fluid parcels near the pseudo-critical point. Comparison of experimental and numerical results confirmed that traditional RANS models cannot reproduce this particular near-critical phenomenon, indicating the limitations of current RANS models in predicting supercritical flow processes.
(4) Based on the law-of-the-wall and some assumptions, we obtained a friction factor correlation applicable to variable property fluids. Combining our own data with existing literature data, a new correlation was obtained to have a higher predicting performance compared with recently proposed correlations, as shown in the following equation. The relative error between 94% of evaluated data and the new correlation falls within ±20%. This correlation is applicable to flow conditions where the relative roughness of the tube ranges from 0 to 0.025 and Re ranges from 3100 to 1.4×10^6.

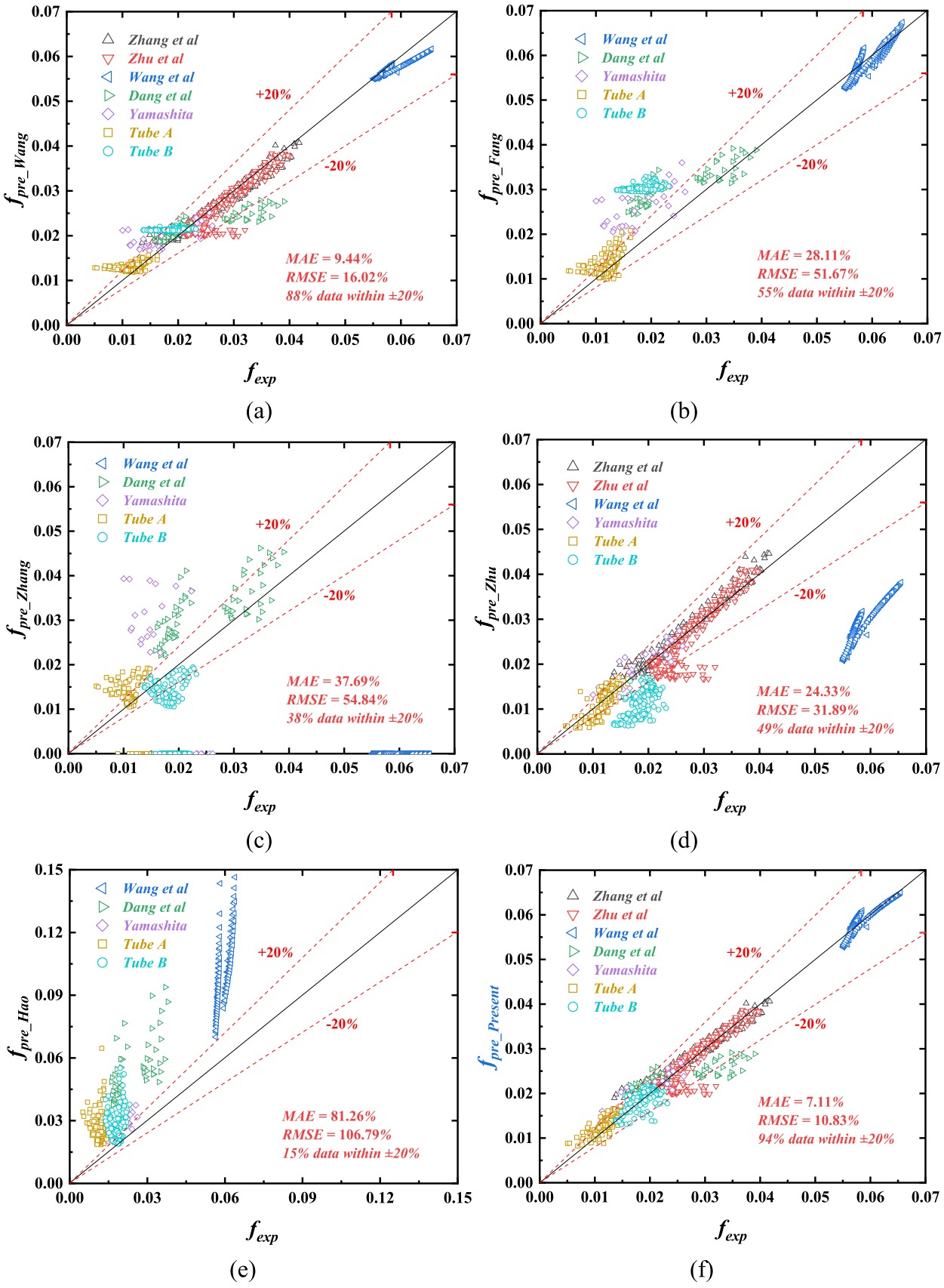

Fig. 16. Comparison of predicted frictional factors of different correlations.

$$f = \left(\frac{\left(\frac{2\rho_b}{\rho_b+\rho_w}\right)^{0.8770} \sqrt{\frac{\rho_w}{\rho_b}}}{1.9856 \cdot \log\left(\mathrm{Re}_w \sqrt{f} \sqrt{\frac{\rho_w}{\rho_b}}\right) + 1.8959 - \frac{31.0299}{\mathrm{Re}_w f} + 3.5981 \cdot \log\left(\frac{\left(1.8495 + \frac{\varepsilon}{d}\mathrm{Re}_w f\right)^{0.3963}}{\mathrm{Re}_w \sqrt{\frac{\rho_w}{\rho_b}}}\right)} \right)^2$$

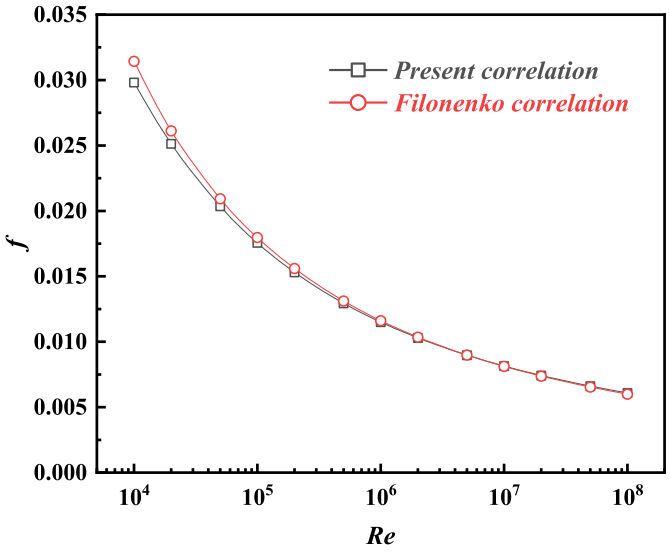

Fig. 17. Comparison between Eq. (22) and the Filonenko correlation.

CRediT authorship contribution statement

Zheng Wang: Conceptualization, Methodology, Investigation, Software, Validation, Data curation, Formal analysis, Visualization, Writing – original draft, Writing – review & editing. **Qinghe Guo:** Investigation, Data curation. **Yi Wu:** Investigation, Data curation. **Zhangquan Wen:** Investigation, Data curation. **Yafei Liu:** Investigation, Data curation. **Dan Chen:** Investigation. **Peiwang Zhu:** Methodology, Project administration, Funding acquisition, Resources, Supervision. **Gang Xiao:** Methodology, Project administration, Supervision, Funding acquisition, Resources, Writing – review & editing.

Declaration of Competing Interest

The authors declare that they have no known competing financial interests or personal relationships that could have appeared to influence the work reported in this paper.

Data availability

We have provided all the original experimental data in the Supplementary Information

Acknowledgment

The authors gratefully acknowledge the support from the National Natural Science Foundation of China (No. 52176207), the Zhejiang Provincial Natural Science Foundation (NO. LR20E060001) and the Fundamental Research Funds for the Central Universities (2022ZFJH04).

Supplementary materials

Supplementary material associated with this article can be found, in the online version, at doi:10.1016/j.ijheatmasstransfer.2023.124634.

References

[1] R.P.F.F. da Silva, T.A.P. Rocha-Santos, A.C. Duarte, Supercritical fluid extraction of bioactive compounds, TrAC Trends Anal. Chem. 76 (2016) 40–51.
[2] W.-w. Liu, B. Zhang, Y.-Z. Li, Y.-M. He, H.-C. Zhang, An environmentally friendly approach for contaminants removal using supercritical CO2 for remanufacturing industry, Appl. Surf. Sci. 292 (2014) 142–148.
[3] B. Dai, C. Liu, S. Liu, D. Wang, Q. Wang, T. Zou, X. Zhou, Life cycle techno-enviro-economic assessment of dual-temperature evaporation transcritical CO2 high-temperature heat pump systems for industrial waste heat recovery, Appl. Therm. Eng. 219 (2023), 119570.
[4] Y. Ahn, S.J. Bae, M. Kim, S.K. Cho, S. Baik, J.I. Lee, J.E. Cha, Review of supercritical CO_2 power cycle technology and current status of research and development, Nucl. Eng. Technol. 47 (6) (2015) 647–661.
[5] R. Allam, S. Martin, B. Forrest, J. Fetvedt, X. Lu, D. Freed, G.W. Brown, T. Sasaki, M. Itoh, J. Manning, Demonstration of the Allam cycle: an update on the development status of a high efficiency supercritical carbon dioxide power process employing full carbon capture, Energy Procedia 114 (2017) 5948–5966.
[6] H. Li, Y. Zhang, W. Bai, Y. Yang, K. Li, W. Gao, L. Zhang, C. Zhang, S. Wu, X. Zhang, Control strategies and dynamic experimental tests on the wide-range and rapid load regulation of a first pilot multi-megawatts fossil-fired supercritical CO2 power system, Energy Convers. Manage. 279 (2023), 116748.
[7] A. Lock, K. Hooman, Z. Guan, A detailed model of direct dry-cooling for the supercritical carbon dioxide Brayton power cycle, Appl. Therm. Eng. 163 (2019), 114390.
[8] D. Wang, B. Yu, J. Hu, L. Chen, J. Shi, J. Chen, Heating performance characteristics of CO_2 heat pump system for electrical vehicle in a cold climate, Int. J. Refrig. 85 (2018) 27–41.
[9] S. Minetto, L. Cecchinato, R. Brignoli, S. Marinetti, A. Rossetti, Water-side reversible CO_2 heat pump for residential application, Int. J. Refrig. 63 (2016) 237–250.
[10] I.L. Pioro, R.B. Duffey, T.J. Dumouchel, Hydraulic resistance of fluids flowing in channels at supercritical pressures (survey), Nucl. Eng. Des. 231 (2) (2004) 187–197.
[11] O. Reynolds, An experimental investigation of the circumstances which determine whether the motion of water shall be direct or sinuous, and of the law of resistance in parallel channels, Philos. Trans. R. Soc. London (174) (1883) 935–982.
[12] H. Blasius, Das aehnlichkeitsgesetz bei reibungsvorgängen in flüssigkeiten. Mitteilungen über Forschungsarbeiten Auf Dem Gebiete des Ingenieurwesens: Insbesondere aus den Laboratorien der Technischen Hochschulen, Springer, 1913, pp. 1–41.
[13] J. Nikuradse, Laws of flow in rough pipes, (1950).
[14] C.F. Colebrook, C.M. White, Experiments with fluid friction in roughened pipes, in: Proceedings of the Royal Society of London. Series A-Mathematical and Physical Sciences 161, 1937, pp. 367–381.
[15] W.F. Durand, Aerodynamic theory: a general review of progress under a grant of the Guggenheim Fund for the Promotion of Aeronautics, (2013).
[16] Z. Wang, B. Sun, J. Wang, L. Hou, Experimental study on the friction coefficient of supercritical carbon dioxide in pipes, Int. J. Greenhouse Gas Control 25 (2014) 151–161.
[17] R.W. Allen, E.R.G. Eckert, Friction and heat-transfer measurements to turbulent pipe flow of water (Pr=7 and 8) at uniform wall heat flux, J. Heat Transf. 86 (3) (1964) 301–310.
[18] A. Carr, M. Connor, H. Buhr, Velocity, temperature, and turbulence measurements in air for pipe flow with combined free and forced convection, J. Heat Transf. 95 (4) (1973) 445–452.
[19] J. Easby, The effect of buoyancy on flow and heat transfer for a gas passing down a vertical pipe at low turbulent Reynolds numbers, Int. J. Heat Mass Transf. 21 (6) (1978) 791–801.
[20] J. Pettersen, R. Rieberer, S.T. Munkejord, Heat Transfer and Pressure Drop for Flow of Supercritical and Subcritical CO_2 in Microchannel Tubes, 5127, Norwegian University of Science and Technology/SINTEF Energy Research, TR A, 2000, p. 2000.

[21] S.M. Liao, T.S. Zhao, Measurements of heat transfer coefficients from supercritical carbon dioxide flowing in horizontal mini/micro channels, J. Heat Transf. 124 (3) (2002) 413–420.
[22] T. Yamashita, H. Mori, S. Yoshida, M. Ohno, Heat Transfer and Pressure Drop of a Supercritical Pressure Fluid Flowing in a Tube of Small Diameter, 63, Memoirs of the Faculty of Engineering Kyushu University, 2003, pp. 227–244.
[23] Y. Jiang, Heat Transfer and Pressure Drop of Refrigerant R404A at Near-Critical and Supercritical Pressures, Iowa State University, 2004.
[24] S.W. Churchill, Comprehensive correlating equations for heat, mass and momentum transfer in fully developed flow in smooth tubes, Ind. Eng. Chem. Fundam. 16 (1) (1977) 109–116.
[25] U.C. Andresen, Supercritical Gas Cooling and Near-Critical-Pressure Condensation of Refrigerant Blends in Microchannels, Georgia Institute of Technology, 2006.
[26] C.-R. Zhao, P.-X. Jiang, Experimental study of in-tube cooling heat transfer and pressure drop characteristics of R134a at supercritical pressures, Exp. Therm Fluid Sci. 35 (7) (2011) 1293–1303.
[27] N. Petrov, V. Popov, Heat-transfer and resistance of carbon-dioxide being cooled in the supercritical region, Therm. Eng. 32 (3) (1985) 131–134.
[28] C. Zhang, G. Xu, H. Deng, K. Zhu, Investigation of flow resistance characteristics of endothermic hydrocarbon fuel under supercritical pressures, Propuls. Power Res. 2 (2) (2013) 119–130.
[29] X. Fang, L. Xu, Y. Chen, W. Chen, Correlations for friction factor of turbulent pipe flow under supercritical pressure: review and a new correlation, Prog. Nucl. Energy 118 (2020), 103085.
[30] H. Zhang, J. Xu, X. Zhu, J. Xie, M. Li, B. Zhu, The K number, a new analogy criterion number to connect pressure drop and heat transfer of sCO_2 in vertical tubes, Appl. Therm. Eng. 182 (2021), 116078.
[31] S.G. Kandlikar, Heat transfer mechanisms during flow boiling in microchannels, J. Heat Transf. 126 (1) (2004) 8–16.
[32] B. Hao, C. Zhang, L. Cheng, J. Xu, Q. Wang, Experimental investigation on the pressure drop characteristics of subcritical and supercritical CO2 heated in a horizontal tube, Int. J. Heat Mass Transf. 201 (2023), 123650.
[33] Q. Wang, X. Ma, J. Xu, M. Li, Y. Wang, The three-regime-model for pseudo-boiling in supercritical pressure, Int. J. Heat Mass Transf. 181 (2021), 121875.
[34] M. Zhu, L. Chen, S. Su, S. Hu, K. Xu, P. Yan, H. Qing, L. Zhou, A. Li, J. Zhou, Flow resistance analysis of non-isothermal supercritical CO_2, Appl. Therm. Eng. 215 (2022), 119022.
[35] G. Filonenko, Hydraulic resistance in pipes, Teploenergetika 1 (1954) 40–44.
[36] C. Dang, K. Iino, K. Fukuoka, E. Hihara, Effect of lubricating oil on cooling heat transfer of supercritical carbon dioxide, Int. J. Refrig. 30 (4) (2007) 724–731.
[37] C.-R. Zhao, P.-X. Jiang, Y.-W. Zhang, Flow and convection heat transfer characteristics of CO_2 mixed with lubricating oil at super-critical pressures in small tube during cooling, Int. J. Refrig. 34 (1) (2011) 29–39.
[38] C.-R. Zhao, Z. Zhang, P.-X. Jiang, Predictions of in-tube cooling heat transfer coefficients and pressure drops of CO_2 and lubricating oil mixture at supercritical pressures, Heat Transfer Eng. 39 (16) (2017) 1437–1449.
[39] F.F. Farshad, T.C. Pesacreta, Coated pipe interior surface roughness as measured by three scanning probe instruments, Anti-Corros. Methods Mater. 50 (1) (2003) 6–16.
[40] T. Adams, C. Grant, H. Watson, A simple algorithm to relate measured surface roughness to equivalent sand-grain roughness, Int. J. Mech. Eng. Mechatron. 1 (2) (2012) 66–71.
[41] W.H. Snyder, I.P. Castro, The critical Reynolds number for rough-wall boundary layers, J. Wind Eng. Ind. Aerodyn. 90 (1) (2002) 41–54.
[42] P.-X. Jiang, Y. Zhang, C.-R. Zhao, R.-F. Shi, Convection heat transfer of CO_2 at supercritical pressures in a vertical mini tube at relatively low reynolds numbers, Exp. Therm Fluid Sci. 32 (8) (2008) 1628–1637.
[43] B.E. Launder, D.B. Spalding, Paper 8 - the numerical computation of turbulent flows, in: S.V. Patankar, A. Pollard, A.K. Singhal, S.P. Vanka (Eds.), Numerical Prediction of Flow, Heat Transfer, Turbulence and Combustion, Pergamon, 1983, pp. 96–116.
[44] V. Yakhot, S.A. Orszag, Renormalization group analysis of turbulence. I. Basic theory, J. Sci. Comput. 1 (1) (1986) 3–51.
[45] T.-H. Shih, W.W. Liou, A. Shabbir, Z. Yang, J. Zhu, A new k-ϵ eddy viscosity model for high reynolds number turbulent flows, Comput. Fluids 24 (3) (1995) 227–238.
[46] F.R. Menter, Two-equation eddy-viscosity turbulence models for engineering applications, AIAA J. 32 (8) (1994) 1598–1605.
[47] Z. Wang, G. Xiao, Y. Liu, Y. Ji, H. Xu, Reference temperature correction and dimensionless number analysis for heat transfer of supercritical CO_2 in horizontal tubes, Int. J. Heat Mass Transf. 194 (2022), 122973.
[48] K. Zhu, G.-Q. Xu, Z. Tao, H.-W. Deng, Z.-H. Ran, C.-B. Zhang, Flow frictional resistance characteristics of kerosene RP-3 in horizontal circular tube at supercritical pressure, Exp. Therm Fluid Sci. 44 (2013) 245–252.
[49] C. Dang, E. Hihara, In-tube cooling heat transfer of supercritical carbon dioxide. Part 1. Experimental measurement, Int. J. Refrig. 27 (7) (2004) 736–747.
[50] S. Garimella, B. Mitra, U.C. Andresen, Y. Jiang, B.M. Fronk, Heat transfer and pressure drop during supercritical cooling of HFC refrigerant blends, Int. J. Heat Mass Transf. 91 (2015) 477–493.
[51] P. Heller, Experimental investigations of critical phenomena, Rep. Prog. Phys. 30 (2) (1967) 731.
[52] P.C. Ma, X.I. Yang, M. Ihme, Structure of wall-bounded flows at transcritical conditions, Phys. Rev. Fluids 3 (3) (2018), 034609.
[53] H. Schlichting, J. Kestin, Boundary Layer Theory, Springer, 1961.